Evidence for exotic hadron contributions to $\Lambda_b^0 \to J/\psi\, p\pi^-$ decays

The LHCb collaboration[†]

Abstract

A full amplitude analysis of $\Lambda_b^0 \to J/\psi\, p\pi^-$ decays is performed with a data sample acquired with the LHCb detector from 7 and 8 TeV pp collisions, corresponding to an integrated luminosity of $3\,\text{fb}^{-1}$. A significantly better description of the data is achieved when, in addition to the previously observed nucleon excitations $N \to p\pi^-$, either the $P_c(4380)^+$ and $P_c(4450)^+ \to J/\psi\, p$ states, previously observed in $\Lambda_b^0 \to J/\psi\, pK^-$ decays, or the $Z_c(4200)^- \to J/\psi\, \pi^-$ state, previously reported in $B^0 \to J/\psi\, K^+\pi^-$ decays, or all three, are included in the amplitude models. The data support a model containing all three exotic states, with a significance of more than three standard deviations. Within uncertainties, the data are consistent with the $P_c(4380)^+$ and $P_c(4450)^+$ production rates expected from their previous observation taking account of Cabibbo suppression.

[†]Authors are listed at the end of this paper.

From the birth of the quark model, it has been anticipated that baryons could be constructed not only from three quarks, but also four quarks and an antiquark [1, 2], hereafter referred to as pentaquarks [3, 4]. The distribution of the $J/\psi p$ mass ($m_{J/\psi p}$) in $\Lambda_b^0 \to J/\psi p K^-$, $J/\psi \to \mu^+\mu^-$ decays (charge conjugation is implied throughout the text) observed with the LHCb detector at the LHC shows a narrow peak suggestive of $uudc\bar{c}$ pentaquark formation, amidst the dominant formation of various excitations of the Λ [uds] baryon (Λ^*) decaying to $K^- p$ [5, 6]. It was demonstrated that these data cannot be described with $K^- p$ contributions alone without a specific model of them [7]. Amplitude model fits were also performed on all relevant masses and decay angles of the six-dimensional data [5], using the helicity formalism and Breit–Wigner amplitudes to describe all resonances. In addition to the previously well-established Λ^* resonances, two pentaquark resonances, named the $P_c(4380)^+$ ($9\,\sigma$ significance) and $P_c(4450)^+$ ($12\,\sigma$), are required in the model for a good description of the data [5]. The mass, width, and fractional yields (fit fractions) were determined to be $4380 \pm 8 \pm 29$ MeV, $205 \pm 18 \pm 86$ MeV, $(8.4 \pm 0.7 \pm 4.3)\%$, and $4450 \pm 2 \pm 3$ MeV, $39 \pm 5 \pm 19$ MeV, $(4.1 \pm 0.5 \pm 1.1)\%$, respectively. Observations of the same two P_c^+ states in another decay would strengthen their interpretation as genuine exotic baryonic states, rather than kinematical effects related to the so-called triangle singularity [8], as pointed out in Ref. [9].

In this Letter, $\Lambda_b^0 \to J/\psi p \pi^-$ decays are analyzed, which are related to $\Lambda_b^0 \to J/\psi p K^-$ decays via Cabibbo suppression. LHCb has measured the relative branching fraction $\mathcal{B}(\Lambda_b^0 \to J/\psi p \pi^-)/\mathcal{B}(\Lambda_b^0 \to J/\psi p K^-) = 0.0824 \pm 0.0024 \pm 0.0042$ [10] with the same data sample as used here, corresponding to $3\,\mathrm{fb}^{-1}$ of integrated luminosity acquired by the LHCb experiment in pp collisions at 7 and 8 TeV center-of-mass energy. The LHCb detector is a single-arm forward spectrometer covering the pseudorapidity range $2 < \eta < 5$, described in detail in Refs. [11, 12]. The data selection is similar to that described in Ref. [5], with the K^- replaced by a π^- candidate. In the preselection a larger significance for the Λ_b^0 flight distance and a tighter alignment between the Λ_b^0 momentum and the vector from the primary to the secondary vertex are required. To remove specific $\overline{B}^0$ and $\overline{B}_s^0$ backgrounds, candidates are vetoed within a $3\,\sigma$ invariant mass window around the corresponding nominal B mass [13] when interpreted as $\overline{B}^0 \to J/\psi \pi^+ K^-$ or as $\overline{B}_s^0 \to J/\psi K^+ K^-$. In addition, residual long-lived $\Lambda \to p\pi^-$ background is excluded if the $p\pi^-$ invariant mass ($m_{p\pi}$) lies within $\pm 5\,\mathrm{MeV}$ of the known Λ mass [13]. The resulting invariant mass spectrum of Λ_b^0 candidates is shown in Fig. 1. The signal yield is 1885 ± 50, determined by an unbinned extended maximum likelihood fit to the mass spectrum. The signal is described by a double-sided Crystal Ball function [14]. The combinatorial background is modeled by an exponential function. The background of $\Lambda_b^0 \to J/\psi p K^-$ events is described by a histogram obtained from simulation, with yield free to vary. This fit is used to assign weights to the candidates using the *sPlot* technique [15], which allows the signal component to be projected out by weighting each event depending on the $J/\psi p \pi^-$ mass. Amplitude fits are performed by minimizing a six-dimensional unbinned negative log-likelihood, $-2\ln\mathcal{L}$, with the background subtracted using these weights and the efficiency folded into the signal probability density function, as discussed in detail in Ref. [5].

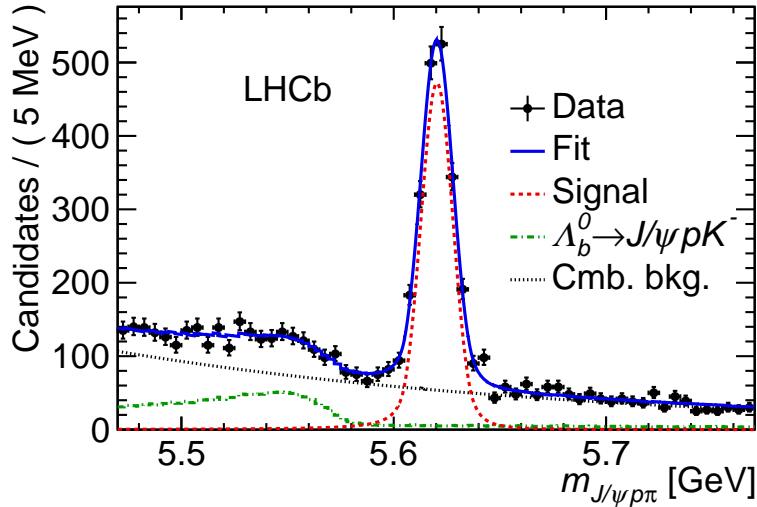Amplitude models for the $\Lambda_b^0 \to J/\psi p \pi^-$ decays are constructed to examine the

Figure 1: Invariant mass spectrum for the selected $\Lambda_b^0 \to J/\psi\, p\pi^-$ candidates.

possibility of exotic hadron contributions from the $P_c(4380)^+$ and $P_c(4450)^+ \to J/\psi\, p$ states and from the $Z_c(4200)^- \to J/\psi\, \pi^-$ state, previously reported by the Belle collaboration in $B^0 \to J/\psi\, K^+\pi^-$ decays [16] (spin-parity $J^P = 1^+$, mass and width of $4196\,^{+31}_{-29}\,^{+17}_{-13}$ MeV and $370 \pm 70\,^{+70}_{-132}$ MeV, respectively). By analogy with kaon decays [17], $p\pi^-$ contributions from conventional nucleon excitations (denoted as N^*) produced with $\Delta I = 1/2$ in Λ_b^0 decays are expected to dominate over Δ excitations with $\Delta I = 3/2$, where I is isospin. The decay matrix elements for the two interfering decay chains, $\Lambda_b^0 \to J/\psi\, N^*$, $N^* \to p\pi^-$ and $\Lambda_b^0 \to P_c^+\pi^-$, $P_c^+ \to J/\psi\, p$ with $J/\psi \to \mu^+\mu^-$ in both cases, are identical to those used in the $\Lambda_b^0 \to J/\psi\, pK^-$ analysis [5], with K^- and Λ^* replaced by π^- and N^*. The additional decay chain, $\Lambda_b^0 \to Z_c^- p$, $Z_c^- \to J/\psi\, \pi^-$, is also included and is discussed in detail in the supplemental material. Helicity couplings, describing the dynamics of the decays, are expressed in terms of LS couplings [5], where L is the decay orbital angular momentum, and S is the sum of spins of the decay products. This is a convenient way to incorporate parity conservation in strong decays and to allow for reduction of the number of free parameters by excluding high L values for phase-space suppressed decays.

Table 1 lists the N^* resonances considered in the amplitude model of $p\pi^-$ contributions. There are 15 well-established N^* resonances [13]. The high-mass and high-spin states ($9/2$ and $11/2$) are not included, since they require $L \geq 3$ in the Λ_b^0 decay and therefore are unlikely to be produced near the upper kinematic limit of $m_{p\pi}$. Theoretical models of baryon resonances predict many more high-mass states [18], which have not yet been observed. Their absence could arise from decreased couplings of the higher N^* excitations to the simple production and decay channels [19] and possibly also from experimental difficulties in identifying broad resonances and insufficient statistics at high masses in scattering experiments. The possibility of high-mass, low-spin N^* states is explored by including two very significant, but unconfirmed, resonances claimed by the BESIII collaboration in $\psi(2S) \to p\bar{p}\pi^0$ decays [20]: $1/2^+$ $N(2300)$ and $5/2^-$ $N(2570)$. A nonresonant $J^P = 1/2^-$

Table 1: The N^* resonances used in the different fits. Parameters are taken from the PDG [13]. The number of LS couplings is listed in the columns to the right for the two versions (RM and EM) of the N^* model discussed in the text. To fix overall phase and magnitude conventions, the $N(1535)$ complex coupling of lowest LS is set to (1,0).

State	J^P	Mass (MeV)	Width (MeV)	RM	EM
NR $p\pi$	$1/2^-$	-	-	4	4
$N(1440)$	$1/2^+$	1430	350	3	4
$N(1520)$	$3/2^-$	1515	115	3	3
$N(1535)$	$1/2^-$	1535	150	4	4
$N(1650)$	$1/2^-$	1655	140	1	4
$N(1675)$	$5/2^-$	1675	150	3	5
$N(1680)$	$5/2^+$	1685	130	-	3
$N(1700)$	$3/2^-$	1700	150	-	3
$N(1710)$	$1/2^+$	1710	100	-	4
$N(1720)$	$3/2^+$	1720	250	3	5
$N(1875)$	$3/2^-$	1875	250	-	3
$N(1900)$	$3/2^+$	1900	200	-	3
$N(2190)$	$7/2^-$	2190	500	-	3
$N(2300)$	$1/2^+$	2300	340	-	3
$N(2570)$	$5/2^-$	2570	250	-	3
Free parameters				40	106

$p\pi^-$ S-wave component is also included. Two models, labeled "reduced" (RM) and "extended" (EM), are considered and differ in the number of resonances and of LS couplings included in the fit as listed in Table 1. The reduced model, used for the central values of fit fractions, includes only the resonances and L couplings that give individually significant contributions. The systematic uncertainties and the significances for the exotic states are evaluated with the extended model by including all well motivated resonances and the maximal number of LS couplings for which the fit is able to converge.

All N^* resonances are described by Breit–Wigner functions [5] to model their lineshape and phase variation as a function of $m_{p\pi}$, except for the $N(1535)$, which is described by a Flatté function [21] to account for the threshold of the $n\eta$ channel. The mass and width are fixed to the values determined from previous experiments [13]. The couplings to the $n\eta$ and $p\pi^-$ channels for the $N(1535)$ state are determined by the branching fractions of the two channels [22]. The nonresonant S-wave component is described with a function that depends inversely on $m_{p\pi}^2$, as this is found to be preferred by the data. An alternative description of the $1/2^-$ $p\pi^-$ contributions, including the $N(1535)$ and nonresonant components, is provided by a K-matrix model obtained from multichannel partial wave analysis by the Bonn–Gatchina group [22,23] and is used to estimate systematic uncertainties.

The limited number of signal events and the large number of free parameters in the

amplitude fits prevent an open-ended analysis of $J/\psi\,p$ and $J/\psi\,\pi^-$ contributions. Therefore, the data are examined only for the presence of the previously observed $P_c(4380)^+$, $P_c(4450)^+$ states [5] and the claimed $Z_c(4200)^-$ resonance [16]. In the fits, the mass and width of each exotic state are fixed to the reported central values. The LS couplings describing $P_c^+ \to J/\psi\,p$ decays are also fixed to the values obtained from the Cabibbo-favored channel. This leaves four free parameters per P_c^+ state for the $\Lambda_b^0 \to P_c^+\pi^-$ couplings. The nominal fits are performed for the most likely $(3/2^-, 5/2^+)$ J^P assignment to the $P_c(4380)^+$, $P_c(4450)^+$ states [5]. All couplings for the 1^+ $Z_c(4200)^-$ contribution are allowed to vary (10 free parameters).

The fits show a significant improvement when exotic contributions are included. When all three exotic contributions are added to the EM N^*-only model, the $\Delta(-2\ln\mathcal{L})$ value is 49.0, which corresponds to their combined statistical significance of $3.9\,\sigma$. Including the systematic uncertainties discussed later lowers their significance to $3.1\,\sigma$. The systematic uncertainties are included in subsequent significance figures. Because of the ambiguity between the $P_c(4380)^+$, $P_c(4450)^+$ and $Z_c(4200)^-$ contributions, no single one of them makes a significant difference to the model. Adding either state to a model already containing the other two, or the two P_c^+ states to a model already containing the $Z_c(4200)^-$ contribution, yields significances below $1.7\,\sigma$ ($0.4\,\sigma$ for adding the $Z_c(4200)^-$ after the two P_c^+ states). If the $Z_c(4200)^-$ contribution is assumed to be negligible, adding the two P_c^+ states to a model without exotics yields a significance of $3.3\,\sigma$. On the other hand, under the assumption that no P_c^+ states are produced, adding the $Z_c(4200)^-$ to a model without exotics yields a significance of $3.2\,\sigma$. The significances are determined using Wilks' theorem [24], the applicability of which has been verified by simulation.

A satisfactory description of the data is already reached with the RM N^* model if either the two P_c^+, or the Z_c^-, or all three states, are included in the fit. The projections of the full amplitude fit onto the invariant masses and the decay angles reasonably well reproduce the data, as shown in Figs. 2–5. The EM N^*-only model does not give good descriptions of the peaking structure in $m_{J/\psi p}$ observed for $m_{p\pi} > 1.8$ GeV (Fig. 3(b)). In fact, all contributions to $\Delta(-2\ln\mathcal{L})$ favoring the exotic components belong to this $m_{p\pi}$ region. The models with the P_c^+ states describe the $m_{J/\psi p}$ peaking structure better than with the $Z_c(4200)^-$ alone (see the supplemental material).

The model with all three exotic resonances is used when determining the fit fractions. The sources of systematic uncertainty are listed in Table 2. They include varying the masses and widths of N^* resonances, varying the masses and widths of the exotic states, considering N^* model dependence and other possible spin-parities J^P for the two P_c^+ states, varying the Blatt–Weisskopf radius [5] between 1.5 and $4.5\,\mathrm{GeV}^{-1}$, changing the angular momenta L in Λ_b^0 decays that are used in the resonant mass description by one or two units, using the K-matrix model for the S-wave $p\pi$ resonances, varying the fixed couplings of the P_c^+ decay by their uncertainties, and splitting Λ_b^0 and J/ψ helicity angles into bins when determining the weights for the background subtraction to account for correlations between the invariant mass of $J/\psi\,p\pi^-$ and these angles. A putative $Z_c(4430)^-$ contribution [16, 25, 26] hardly improves the value of $-2\ln\mathcal{L}$ relative to the EM N^*-only model, and thus is considered among systematic uncertainties. Exclusion of the $Z_c(4200)^-$
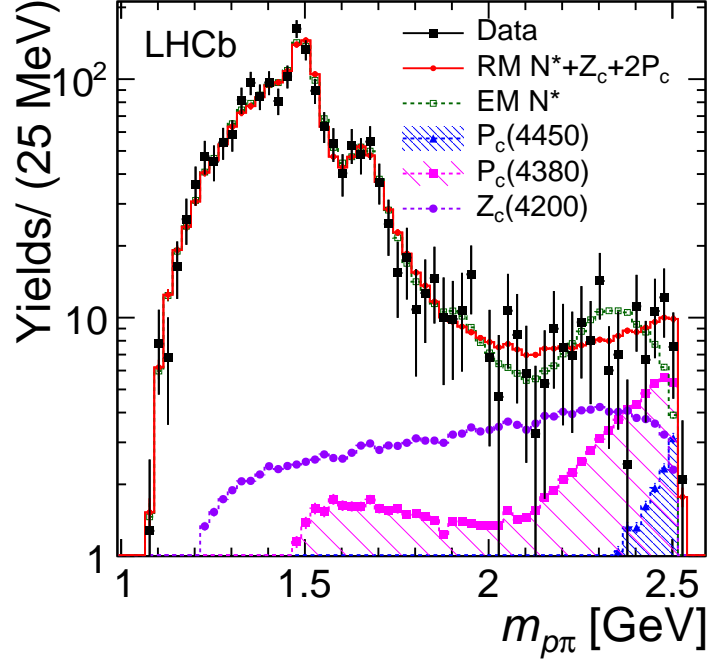
Figure 2: Background-subtracted data and fit projections onto $m_{p\pi}$. Fits are shown with models containing N^* states only (EM) and with N^* states (RM) plus exotic contributions.
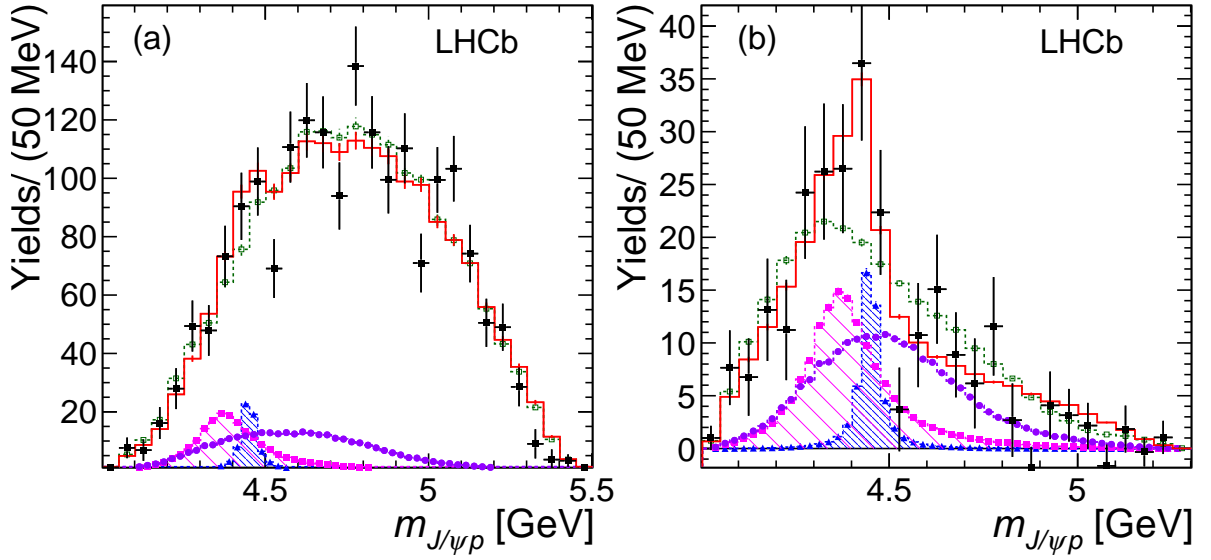

Figure 3: Background-subtracted data and fit projections onto $m_{J/\psi p}$ for (a) all events and (b) the $m_{p\pi} > 1.8$ GeV region. See the legend and caption of Fig. 2 for a description of the components.
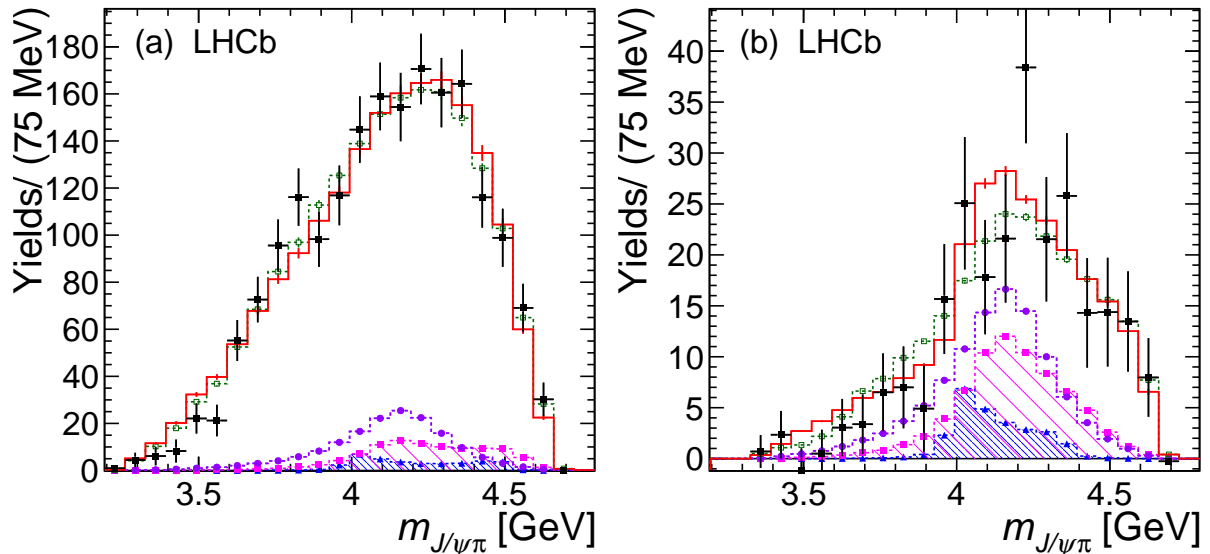
Figure 4: Background-subtracted data and fit projections onto $m_{J/\psi\pi}$ for (a) all events and (b) the $m_{p\pi} > 1.8$ GeV region. See the legend and caption of Fig. 2 for a description of the components.

state from the fit model is also considered to determine the systematic uncertainties for the two P_c^+ states.

The EM model is used to assess the uncertainty due to the N^* modeling when computing significances. The RM model gives larger significances. All sources of systematic uncertainties, including the ambiguities in the quantum number assignments to the two P_c^+ states, are accounted for in the calculation of the significance of various contributions, by using the smallest $\Delta(-2\ln\mathcal{L})$ among the fits representing different systematic variations.

The fit fractions for the $P_c(4380)^+$, $P_c(4450)^+$ and $Z_c(4200)^-$ states are measured to be $(5.1 \pm 1.5\,^{+2.6}_{-1.6})\%$, $(1.6\,^{+0.8}_{-0.6}\,^{+0.6}_{-0.5})\%$, and $(7.7 \pm 2.8\,^{+3.4}_{-4.0})\%$ respectively, and to be less than 8.9%, 2.9%, and 13.3% at 90% confidence level, respectively. When the two P_c^+ states are not considered, the fraction for the $Z_c(4200)^-$ state is surprisingly large, $(17.2 \pm 3.5)\%$, where the uncertainty is statistical only, given that its fit fraction was measured to be only $(1.9\,^{+0.7}_{-0.5}\,^{+0.9}_{-0.5})\%$ in $B^0 \to J/\psi K^+\pi^-$ decays [16]. Conversely, the fit fractions of the two P_c^+ states remain stable regardless of the inclusion of the $Z_c(4200)^-$ state. We measure the relative branching fraction $R_{\pi/K} \equiv \mathcal{B}(\Lambda_b^0 \to \pi^- P_c^+)/\mathcal{B}(\Lambda_b^0 \to K^- P_c^+)$ to be $0.050 \pm 0.016\,^{+0.026}_{-0.016} \pm 0.025$ for $P_c(4380)^+$ and $0.033\,^{+0.016}_{-0.014}\,^{+0.011}_{-0.010} \pm 0.009$ for $P_c(4450)^+$, respectively, where the first error is statistical, the second is systematic, and the third is due to the systematic uncertainty on the fit fractions of the P_c^+ states in $J/\psi pK^-$ decays. The results are consistent with a prediction of (0.07–0.08) [27], where the assumption is made that an additional diagram with internal W emission, which can only contribute to the Cabibbo-suppressed mode, is negligible. Our measurement rules out the proposal that the P_c^+ state in the $\Lambda_b^0 \to J/\psi pK^-$ decay is produced mainly by the charmless Λ_b^0 decay via

Table 2: Summary of absolute systematic uncertainties of the fit fractions in units of percent.

Source	$P_c(4450)^+$	$P_c(4380)^+$	$Z_c(4200)^-$
N^* masses and widths	±0.05	±0.23	±0.31
P_c^+, Z_c^- masses and widths	±0.32	±1.27	±1.56
Additional N^*	$+0.08 \atop -0.23$	$+0.59 \atop -0.55$	$+0.71 \atop -2.92$
Inclusion of $Z_c(4430)^-$	$+0.01$	$+0.97$	$+2.87$
Exclusion of $Z_c(4200)^-$	-0.15	$+1.61$	-
Other J^P	$+0.38 \atop -0.00$	$+0.92 \atop -0.28$	$+0.00 \atop -2.16$
Blatt–Weisskopf radius	±0.11	±0.17	±0.21
$L_{\Lambda_b^0}^{N^*}$ in $\Lambda_b^0 \to J/\psi\, N^*$	±0.07	±0.46	±0.04
$L_{\Lambda_b^0}^{P_c}$ in $\Lambda_b^0 \to P_c^+\pi^-$	-0.05	-0.17	$+0.09$
$L_{\Lambda_b^0}^{Z_c}$ in $\Lambda_b^0 \to Z_c^- p$	±0.07	±0.22	±0.53
K-matrix model	-0.03	$+0.11$	-0.02
P_c^+ couplings	±0.14	±0.31	±0.36
Background subtraction	-0.07	-0.13	-0.39
Total	$+0.55 \atop -0.48$	$+2.61 \atop -1.58$	$+3.43 \atop -4.04$

the $b \to u\bar{u}s$ transition, since this predicts a very large value for $R_{\pi/K} = 0.58 \pm 0.05$ [28].

In conclusion, we have performed a full amplitude fit to $\Lambda_b^0 \to J/\psi\, p\pi^-$ decays allowing for previously observed conventional ($p\pi^-$) and exotic ($J/\psi\, p$ and $J/\psi\, \pi^-$) resonances. A significantly better description of the data is achieved by either including the two P_c^+ states observed in $\Lambda_b^0 \to J/\psi\, pK^-$ decays [5], or the $Z_c(4200)^-$ state reported by the Belle collaboration in $B^0 \to J/\psi\, \pi^- K^+$ decays [16]. If both types of exotic resonances are included, the total significance for them is $3.1\,\sigma$. Individual exotic hadron components, or the two P_c^+ states taken together, are not significant as long as the other(s) is (are) present. Within the statistical and systematic errors, the data are consistent with the $P_c(4380)^+$ and $P_c(4450)^+$ production rates expected from their previous observation and Cabibbo suppression. Assuming that the $Z_c(4200)^-$ contribution is negligible, there is a $3.3\,\sigma$ significance for the two P_c^+ states taken together.
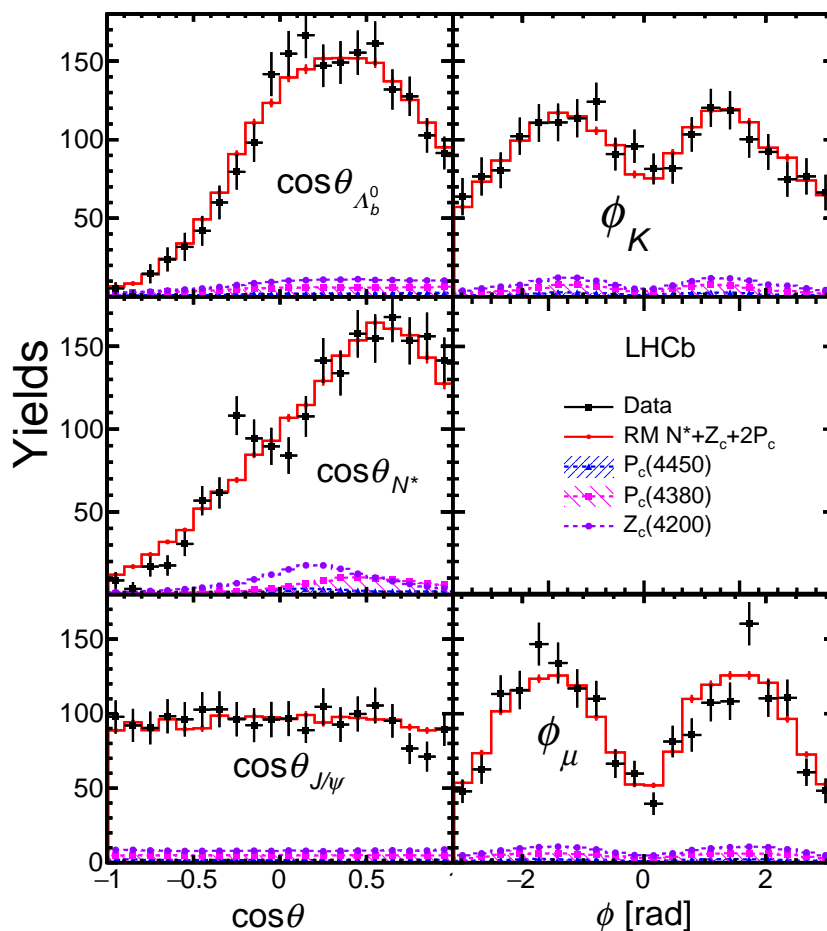
Figure 5: Background-subtracted data and fit projections of decay angles describing the N^* decay chain, which are included in the amplitude fit. The helicity angle of particle P, θ_P, is the polar angle in the rest frame of P between a decay product of P and the boost direction from the particle decaying to P. The azimuthal angle between decay planes of Λ_b^0 and N^* (of J/ψ) is denoted as ϕ_π (ϕ_μ). See Ref. [5] for more details.

References

[1] M. Gell-Mann, *A schematic model of baryons and mesons*, Phys. Lett. **8** (1964) 214.

[2] G. Zweig, *An SU_3 model for strong interaction symmetry and its breaking*, CERN-TH-401, 1964.

[3] L. Montanet, G. C. Rossi, and G. Veneziano, *Baryonium physics*, Phys. Rep. **63** (1980) 151.

[4] H. J. Lipkin, *New possibilities for exotic hadrons: Anticharmed strange baryons*, Phys. Lett. **B195** (1987) 484.

[5] LHCb collaboration, R. Aaij *et al.*, *Observation of $J/\psi p$ resonances consistent with pentaquark states in $\Lambda_b^0 \to J/\psi p K^-$ decays*, Phys. Rev. Lett. **115** (2015) 072001, `arXiv:1507.03414`.

[6] LHCb collaboration, R. Aaij *et al.*, *Study of the productions of Λ_b^0 and $\overline{B}^0$ hadrons in pp collisions and first measurement of the $\Lambda_b^0 \to J/\psi p K^-$ branching fraction*, Chin. Phys. C **40** (2016) 011001, `arXiv:1509.00292`.

[7] LHCb collaboration, R. Aaij *et al.*, *Model-independent evidence for $J/\psi p$ contributions to $\Lambda_b^0 \to J/\psi p K^-$ decays*, Phys. Rev. Lett. **117** (2016) 082002, `arXiv:1604.05708`.

[8] F.-K. Guo, U.-G. Meiner, W. Wang, and Z. Yang, *How to reveal the exotic nature of the $P_c(4450)$*, Phys. Rev. **D92** (2015) 071502, `arXiv:1507.04950`; X.-H. Liu, Q. Wang, and Q. Zhao, *Understanding the newly observed heavy pentaquark candidates*, Phys. Lett. **B757** (2016) 231, `arXiv:1507.05359`; M. Mikhasenko, *A triangle singularity and the LHCb pentaquarks*, `arXiv:1507.06552`.

[9] T. J. Burns, *Phenomenology of $P_c(4380)^+$, $P_c(4450)^+$ and related states*, Eur. Phys. J. **A51** (2015) 152, `arXiv:1509.02460`; E. Wang *et al.*, *Hidden-charm pentaquark state in $\Lambda_b^0 \to J/\psi p \pi^-$ decay*, Phys. Rev. **D93** (2016) 094001, `arXiv:1512.01959`.

[10] LHCb collaboration, R. Aaij *et al.*, *Observation of the $\Lambda_b^0 \to J/\psi p \pi^-$ decay*, JHEP **07** (2014) 103, `arXiv:1406.0755`.

[11] LHCb collaboration, A. A. Alves Jr. *et al.*, *The LHCb detector at the LHC*, JINST **3** (2008) S08005.

[12] LHCb collaboration, R. Aaij *et al.*, *LHCb detector performance*, Int. J. Mod. Phys. **A30** (2015) 1530022, `arXiv:1412.6352`.

[13] Particle Data Group, K. A. Olive *et al.*, *Review of particle physics*, Chin. Phys. **C38** (2014) 090001.

[14] T. Skwarnicki, *A study of the radiative cascade transitions between the Upsilon-prime and Upsilon resonances*, PhD thesis, Institute of Nuclear Physics, Krakow, 1986, DESY-F31-86-02.

[15] M. Pivk and F. R. Le Diberder, *sPlot: A statistical tool to unfold data distributions*, Nucl. Instrum. Meth. **A555** (2005) 356, `arXiv:physics/0402083`.

[16] Belle collaboration, K. Chilikin *et al.*, *Observation of a new charged charmoniumlike state in $\bar{B}^0 \to J/\psi K^- \pi^+$ decays*, Phys. Rev. **D90** (2014) 112009, `arXiv:1408.6457`.

[17] J. F. Donoghue, E. Golowich, W. A. Ponce, and B. R. Holstein, *Analysis of $\Delta S{=}1$ nonleptonic weak decays and the $\Delta I{=}1/2$ rule*, Phys. Rev. **D21** (1980) 186.

[18] U. Loring, B. C. Metsch, and H. R. Petry, *The light baryon spectrum in a relativistic quark model with instanton induced quark forces: The nonstrange baryon spectrum and ground states*, Eur. Phys. J. **A10** (2001) 395, `arXiv:hep-ph/0103289`.

[19] R. Koniuk and N. Isgur, *Where have all the resonances gone? An analysis of baryon couplings in a quark model with chromodynamics*, Phys. Rev. Lett. **44** (1980) 845.

[20] BESIII collaboration, M. Ablikim *et al.*, *Observation of two new N^* resonances in the decay $\psi(3686) \to p\bar{p}\pi^0$*, Phys. Rev. Lett. **110** (2013) 022001, `arXiv:1207.0223`.

[21] S. M. Flatté, *Coupled-channel analysis of the $\pi\eta$ and $K\overline{K}$ systems near $K\overline{K}$ threshold*, Phys. Lett. **B63** (1976) 224.

[22] A. V. Anisovich *et al.*, *Properties of baryon resonances from a multichannel partial wave analysis*, Eur. Phys. J. **A48** (2012) 15, `arXiv:1112.4937`.

[23] A. V. Anisovich *et al.*, *Photoproduction of pions and properties of baryon resonances from a Bonn-Gatchina partial wave analysis*, Eur. Phys. J. **A44** (2010) 203, `arXiv:0911.5277`.

[24] S. S. Wilks, *The large-sample distribution of the likelihood ratio for testing composite hypotheses*, Ann. Math. Stat. **9** (1938) 60.

[25] Belle collaboration, K. Chilikin *et al.*, *Experimental constraints on the spin and parity of the $Z(4430)^+$*, Phys. Rev. **D88** (2013) 074026, `arXiv:1306.4894`.

[26] LHCb collaboration, R. Aaij *et al.*, *Observation of the resonant character of the $Z(4430)^-$ state*, Phys. Rev. Lett. **112** (2014) 222002, `arXiv:1404.1903`; LHCb collaboration, R. Aaij *et al.*, *A model-independent confirmation of the $Z(4430)^-$ state*, Phys. Rev. **D92** (2015) 112009, `arXiv:1510.01951`.

[27] H.-Y. Cheng and C.-K. Chua, *Bottom baryon decays to pseudoscalar meson and pentaquark*, Phys. Rev. **D92** (2015) 096009, `arXiv:1509.03708`.

[28] Y. K. Hsiao and C. Q. Geng, *Pentaquarks from intrinsic charms in Λ_b^0 decays*, Phys. Lett. **B751** (2015) 572, `arXiv:1508.03910`.

Appendix: Supplemental material

Contents

1 Dalitz plot distributions

In Fig. 6, we show the Dalitz plots using the invariant mass squared, $m^2_{p\pi}$ vs $m^2_{J/\psi p}$, and $m^2_{p\pi}$ vs $m^2_{J/\psi \pi}$ as independent variables. As expected, significant N^* contributions are seen, especially in the region around $m^2_{p\pi} \approx 2\,\mathrm{GeV}^2$. There is no visible narrow band around the $P_c(4450)$ region at about $20\,\mathrm{GeV}^2$ in the $J/\psi p$ mass-squared. However many events concentrate in a limited window around $m^2_{p\pi} = 6\,\mathrm{GeV}^2$ and $m^2_{J/\psi p}$ between 18 to 20 GeV^2, which could be due to the P_c contribution. Distributions of efficiency and background on the Dalitz plane are shown in Fig. 7, where the background consists of events from the Λ^0_b candidate mass sideband of $5665 - 5770\,\mathrm{MeV}$. The efficiency is obtained from MC simulation with data-driven corrections applied for the particle identification of the pion and proton.

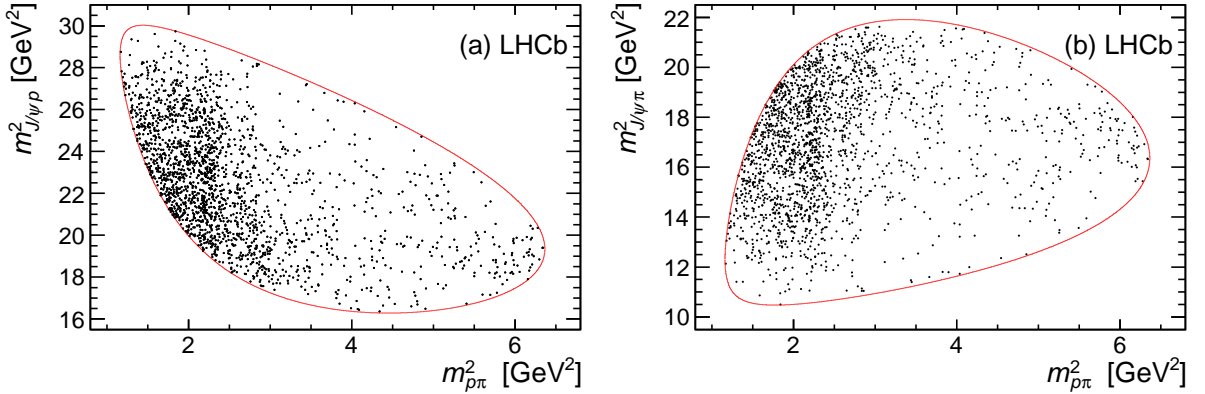Figure 6: Invariant mass squared of $p\pi^-$ versus either (a) $J/\psi p$ or (b) $J/\psi \pi$ for candidates within $\pm 15\,\mathrm{MeV}$ of the Λ^0_b mass, which contain 17% background. The lines show the kinematic boundaries with the Λ^0_b mass constrained to the known value.
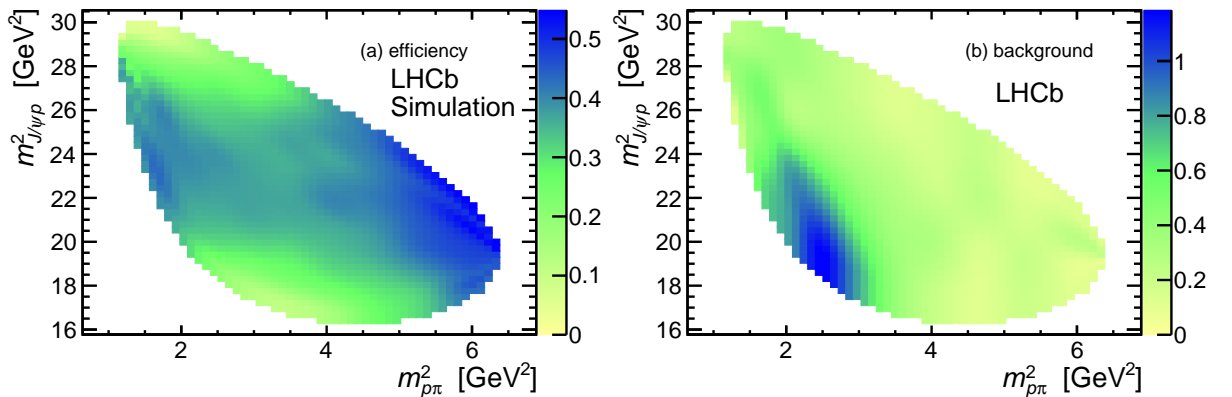

Figure 7: (a) Relative signal efficiency and (b) background distribution on the Dalitz plane in arbitrary units.
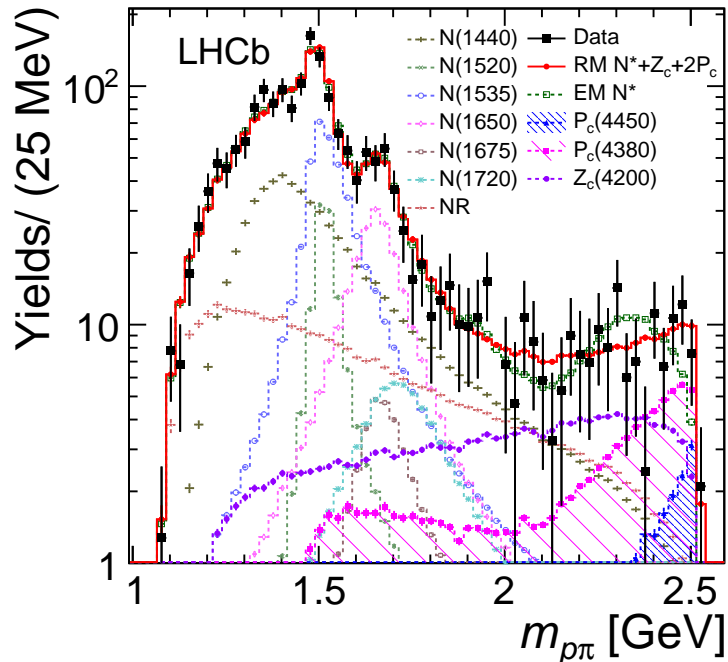
Figure 8: Background-subtracted data and fit projections onto $m_{p\pi}$. Fits are shown with models containing N^* states only (EM) and with N^* states (RM) plus exotic contributions. Individual fit components are shown only for the fit which includes all three exotic resonances.

2 Additional fit results

2.1 Additional fit displays

Figure 8 shows the $m_{p\pi}$ distribution with all individual fit components overlaid. In Fig. 9 we show the same $m_{p\pi}$ distribution but with a linear scale. The projections from the reduced model fit with the two P_c^+ states are shown in Figs. 10–12. The projections from the reduced model fit with the $Z_c(4200)^-$ state are shown in Figs. 13–15. The models with the P_c^+ states describe the $m_{J/\psi p}$ peaking structure better than with the $Z_c(4200)^-$ alone; the $m_{J/\psi p}$ distribution is better described in Fig. 11 (b) than that in Fig. 14 (b).

2.2 Fit fractions

The fit fraction of any component R is defined as $f_R = \int |\mathcal{M}_R|^2 \, \mathrm{d}\Phi / \int |\mathcal{M}|^2 \, \mathrm{d}\Phi$, where $\mathcal{M}_R$ is the matrix element, $\mathcal{M}$, with all except the R amplitude terms are set to zero. The phase space volume $\mathrm{d}\Phi$ is equal to $p \, q \, \mathrm{d}m_{p\pi} \, \mathrm{d}\cos\theta_{\Lambda_b^0} \, \mathrm{d}\cos\theta_{N^*} \, \mathrm{d}\cos\theta_{J/\psi} \, \mathrm{d}\phi_\pi \, \mathrm{d}\phi_\mu$, where p is the momentum of the $p\pi$ system (*i.e.* N^*) in the Λ_b^0 rest frame, and q is the momentum of π^- in the N^* rest frame. In Table 3, we show the fit fractions from the "reduced" and "extended" model fits.

Figure 9: Background-subtracted data and fit projections onto $m_{p\pi}$. Fits are shown with models containing N^* states only (EM) and with N^* states (RM) plus exotic contributions. Individual fit components are shown only for the fit which includes all three exotic resonances.
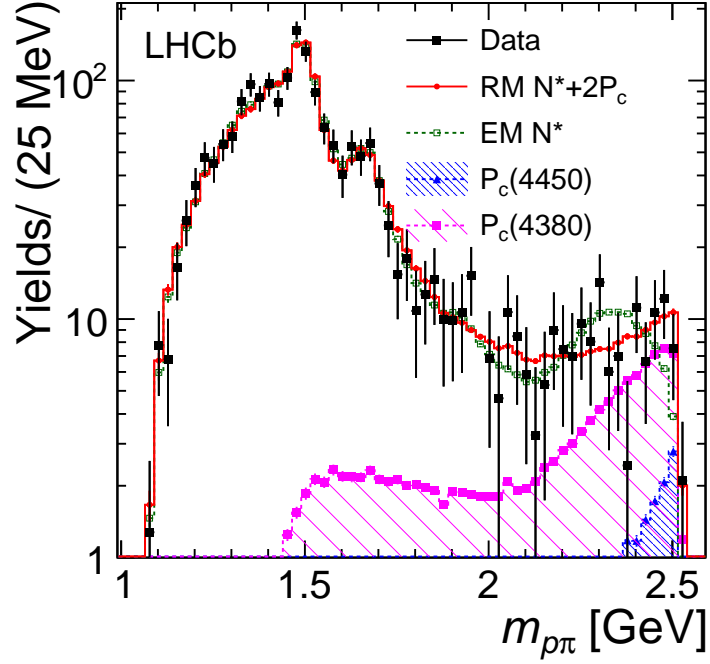
Figure 10: Background-subtracted data and fit projections onto $m_{p\pi}$. Fits are shown with models containing N^* states only (EM) and with N^* states (RM) plus the two P_c^+ resonances.
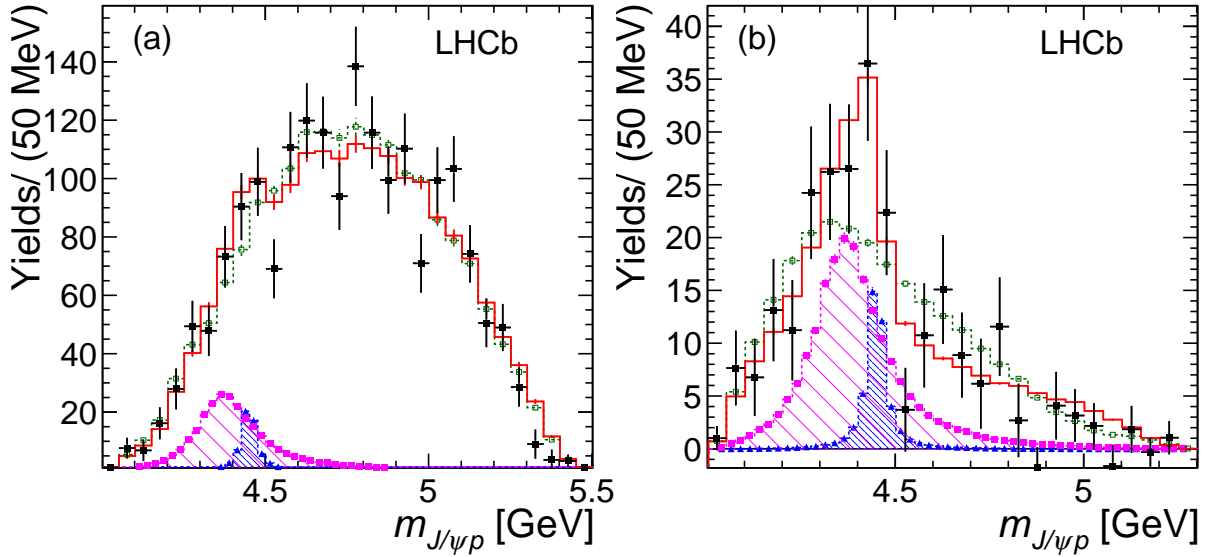
Figure 11: Background-subtracted data and fit projections onto $m_{J/\psi p}$ for (a) all events and (b) the $m_{p\pi} > 1.8$ GeV region. See the legend and caption of Fig. 10 for a description of the components.

15
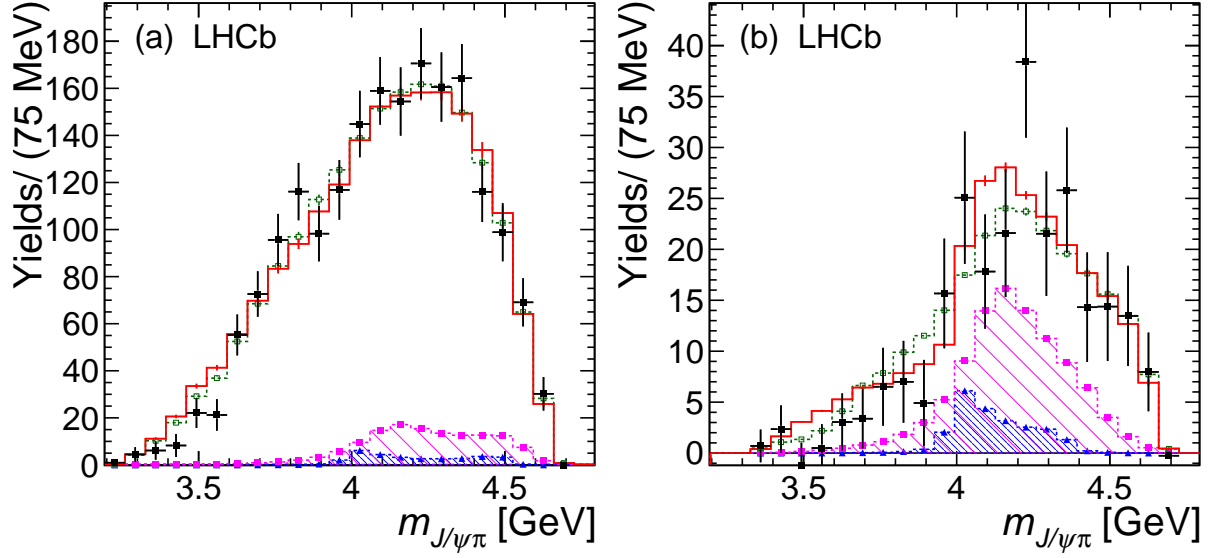
Figure 12: Background-subtracted data and fit projections onto $m_{J/\psi\pi}$ for (a) all events and (b) the $m_{p\pi} > 1.8$ GeV region. See the legend and caption of Fig. 10 for the description.
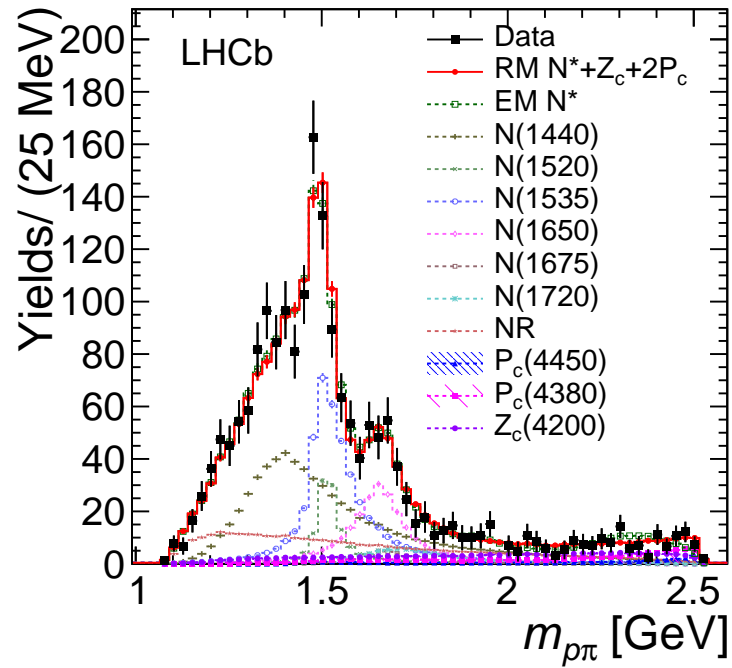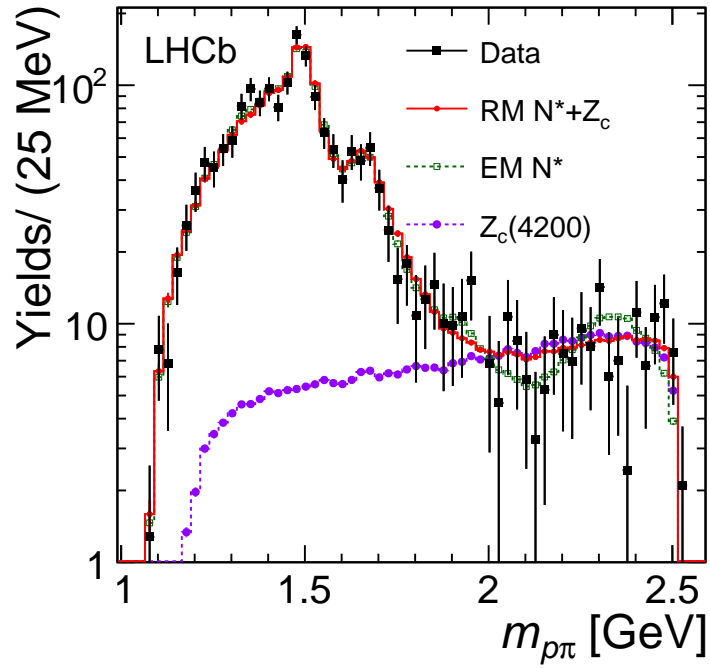

Figure 13: Background-subtracted data and fit projections onto $m_{p\pi}$. Fits are shown with models containing N^* states only (EM) and with N^* states (RM) plus the $Z_c(4200)^-$ resonance.
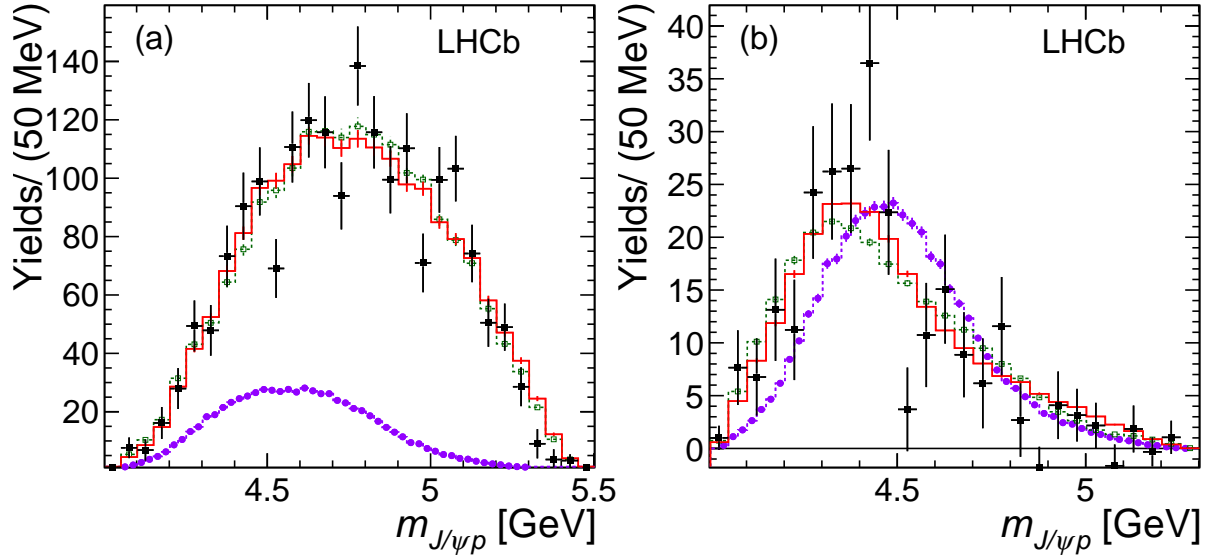
Figure 14: Background-subtracted data and fit projections onto $m_{J/\psi p}$ for (a) all events and (b) the $m_{p\pi} > 1.8$ GeV region. See the legend and caption of Fig. 13 for a description of the components.
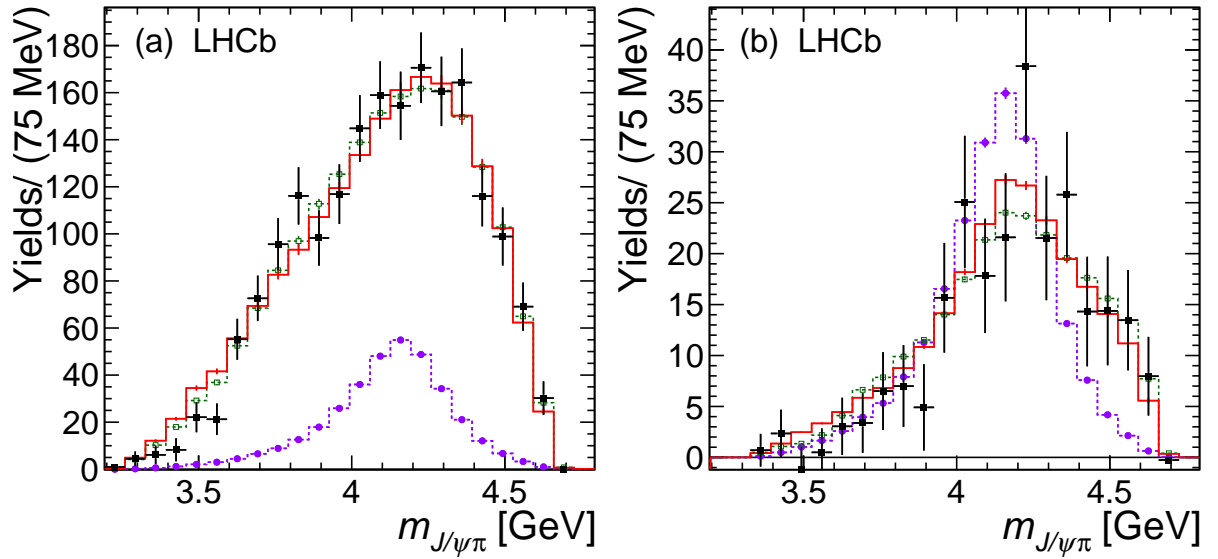
Figure 15: Background-subtracted data and fit projections onto $m_{J/\psi \pi}$ for (a) all events and (b) the $m_{p\pi} > 1.8$ GeV region. See the legend and caption of Fig. 13 for a description of the components.

Table 3: Fit fractions (%) from the RM and EM model fits with statistical uncertainties only.

| State	RM	EM
NR $p\pi$	18.6 ± 3.2	16.0 ± 3.3
$N(1440)$	34.0 ± 4.9	43.9 ± 5.7
$N(1520)$	7.6 ± 2.2	1.9 ± 3.9
$N(1535)$	25.4 ± 5.9	34.4 ± 6.5
$N(1650)$	10.5 ± 5.1	9.5 ± 4.1
$N(1675)$	$3.4 \,^{+2.2}_{-1.0}$	4.2 ± 1.6
$N(1680)$	-	3.0 ± 1.6
$N(1700)$	-	1.7 ± 3.0
$N(1710)$	-	2.1 ± 1.6
$N(1720)$	$3.9 \,^{+1.8}_{-1.3}$	9.6 ± 3.2
$N(1875)$	-	2.3 ± 1.9
$N(1900)$	-	3.0 ± 1.7
$N(2190)$	-	0.5 ± 0.4
$N(2300)$	-	4.9 ± 2.2
$N(2570)$	-	0.3 ± 0.5
$P_c(4380)$	5.1 ± 1.5	4.1 ± 1.7
$P_c(4450)$	$1.6 \,^{+0.8}_{-0.6}$	$1.5 \,^{+0.8}_{-0.6}$
$Z_c(4200)$	7.7 ± 2.8	$4.1 \,^{+4.3}_{-1.1}$

3 Details of the matrix element for the decay amplitude

3.1 Helicity formalism and notation

For each two-body decay $A \to B\,C$, a coordinate system is set up in the rest frame of A, with $\hat{z}$ being[1] the direction of quantization for its spin. We denote this coordinate system as $(x_0^{\{A\}}, y_0^{\{A\}}, z_0^{\{A\}})$, where the superscript "$\{A\}$" means "in the rest frame of A", while the subscript "0" means the initial coordinates. For the first particle in the decay chain (Λ_b^0), the choice of these coordinates is arbitrary.[2] However, once defined, these coordinates must be used consistently between all decay sequences described by the matrix element. For subsequent decays, $e.g.$ $B \to D\,E$, the choice of these coordinates is already fixed by the transformation from the A to the B rest frames, as discussed below. Helicity is defined as the projection of the spin of the particle onto the direction of its momentum. When the z axis coincides with the particle momentum, we denote its spin projection onto it ($i.e.$ the m_z quantum number) as λ. To use the helicity formalism, the initial coordinate system must be rotated to align the z axis with the direction of the momentum of one of the child particles, $e.g.$ the B. A generalized rotation operator can be formulated in three-dimensional space, $\mathcal{R}(\alpha, \beta, \gamma)$, that uses Euler angles. Applying this operator results in a sequence of rotations: first by the angle α about the $\hat{z}_0$ axis, followed by the angle β about the rotated $\hat{y}_1$ axis and then finally by the angle γ about the rotated $\hat{z}_2$ axis. We use a subscript denoting the axes, to specify the rotations which have been already performed on the coordinates. The spin eigenstates of particle A, $|J_A, m_A\rangle$, in the $(x_0^{\{A\}}, y_0^{\{A\}}, z_0^{\{A\}})$ coordinate system can be expressed in the basis of its spin eigenstates, $|J_A, m'_A\rangle$, in the rotated $(x_3^{\{A\}}, y_3^{\{A\}}, z_3^{\{A\}})$ coordinate system with the help of Wigner's D-matrices

$$|J_A, m_A\rangle = \sum_{m'_A} D^{J_A}_{m_A, m'_A}(\alpha, \beta, \gamma)^* |J_A, m'_A\rangle, \tag{1}$$

where

$$D^{J}_{m, m'}(\alpha, \beta, \gamma)^* = \langle J, m|\mathcal{R}(\alpha, \beta, \gamma)|J, m'\rangle^* = e^{i\,m\alpha}\, d^{J}_{m,m'}(\beta)\, e^{i\,m'\gamma}, \tag{2}$$

and where the small-d Wigner matrix contains known functions of β that depend on J, m, m'. To achieve the rotation of the original $\hat{z}_0^{\{A\}}$ axis onto the B momentum $(\vec{p}_B^{\{A\}})$, it is sufficient to rotate by $\alpha = \phi_B^{\{A\}}$, $\beta = \theta_B^{\{A\}}$, where $\phi_B^{\{A\}}$, $\theta_B^{\{A\}}$ are the azimuthal and polar angles of the B momentum vector in the original coordinates $i.e.$ $(\hat{x}_0^{\{A\}}, \hat{y}_0^{\{A\}}, \hat{z}_0^{\{A\}})$. This is depicted in Fig. 16, for the case when the quantization axis for the spin of A is its momentum in some other reference frame. Since the third rotation is not necessary, we set $\gamma = 0$.[3] The angle $\theta_B^{\{A\}}$ is usually called "the A helicity angle", thus to simplify the

---

[1] The "hat" symbol denotes a unit vector in a given direction.

[2] When designing an analysis to be sensitive (or insensitive) to a particular case of polarization, the choice is not arbitrary, but this does not change the fact that one can quantize the Λ_b^0 spin along any well-defined direction. The Λ_b^0 polarization may be different for different choices.

[3] An alternate convention is to set $\gamma = -\alpha$. The two conventions lead to equivalent formulae.

notation we will denote it as θ_A. For compact notation, we will also denote $\phi_B^{\{A\}}$ as ϕ_B. These angles can be determined from[4]

$$\phi_B = \operatorname{atan2}\left(p_B^{\{A\}}{}_y, \; p_B^{\{A\}}{}_x\right)$$
$$= \operatorname{atan2}\left(\hat{y}_0^{\{A\}} \cdot \vec{p}_B^{\{A\}}, \; \hat{x}_0^{\{A\}} \cdot \vec{p}_B^{\{A\}}\right)$$
$$= \operatorname{atan2}\left((\hat{z}_0^{\{A\}} \times \hat{x}_0^{\{A\}}) \cdot \vec{p}_B^{\{A\}}, \; \hat{x}_0^{\{A\}} \cdot \vec{p}_B^{\{A\}}\right), \tag{3}$$
$$\cos\theta_A = \hat{z}_0^{\{A\}} \cdot \hat{p}_B^{\{A\}}. \tag{4}$$

Angular momentum conservation requires $m'_A = m'_B + m'_C = \lambda_B - \lambda_C$ (since $\vec{p}_C^{\{A\}}$ points in the opposite direction to $\hat{z}_3^{\{A\}}$, $m'_C = -\lambda_C$). Each two-body decay contributes a multiplicative term to the matrix element

$$\mathcal{H}_{\lambda_B, \lambda_C}^{A \to B C} \, D_{m_A, \lambda_B - \lambda_C}^{J_A}(\phi_B, \theta_A, 0)^*. \tag{5}$$

The helicity couplings $\mathcal{H}_{\lambda_B, \lambda_C}^{A \to B C}$ are complex constants. Their products from subsequent decays are to be determined by the fit to the data (they represent the decay dynamics). If the decay is strong or electromagnetic, it conserves parity which reduces the number of independent helicity couplings via the relation

$$\mathcal{H}_{-\lambda_B, -\lambda_C}^{A \to B C} = P_A \, P_B \, P_C \, (-1)^{J_B + J_C - J_A} \, \mathcal{H}_{\lambda_B, \lambda_C}^{A \to B C}, \tag{6}$$

where P stands for the intrinsic parity of a particle.

After multiplying terms given by Eq. (5) for all decays in the decay sequence, they must be summed up coherently over the helicity states of intermediate particles, and incoherently over the helicity states of the initial and final-state particles. Possible helicity values of B and C particles are constrained by $|\lambda_B| \le J_B$, $|\lambda_C| \le J_C$ and $|\lambda_B - \lambda_C| \le J_A$.

When dealing with the subsequent decay of the child, $B \to D E$, four-vectors of all particles must be first Lorentz boosted to the rest frame of B, along the $\vec{p}_B^{\{A\}}$ i.e. $\hat{z}_3^{\{A\}}$ direction (this is the z axis in the rest frame of A after the Euler rotations; we use the subscript "3" for the number of rotations performed on the coordinates, because of the three Euler angles, however, since we use the $\gamma = 0$ convention these coordinates are the same as after the first two rotations). This is visualized in Fig. 16, with $B \to D E$ particle labels replaced by $A \to B C$ labels. This transformation does not change vectors that are perpendicular to the boost direction. The transformed coordinates become the initial coordinate system quantizing the spin of B in its rest frame,

$$\hat{x}_0^{\{B\}} = \hat{x}_3^{\{A\}},$$
$$\hat{y}_0^{\{B\}} = \hat{y}_3^{\{A\}},$$
$$\hat{z}_0^{\{B\}} = \hat{z}_3^{\{A\}}. \tag{7}$$

---

[4]The function $\operatorname{atan2}(x, y)$ is the $\tan^{-1}(y/x)$ function with two arguments. The purpose of using two arguments instead of one is to gather information on the signs of the inputs in order to return the appropriate quadrant of the computed angle.

The processes of rotation and subsequent boosting can be repeated until the final-state particles are reached. In practice, there are two equivalent ways to determine the $\hat{z}_0^{\{B\}}$ direction. Using Eq. (7) we can set it to the direction of the B momentum in the A rest frame

$$\hat{z}_0^{\{B\}} = \hat{z}_3^{\{A\}} = \hat{p}_B^{\{A\}}. \tag{8}$$

Alternatively, we can make use of the fact that B and C are back-to-back in the rest frame of A, $\vec{p}_C^{\{A\}} = -\vec{p}_B^{\{A\}}$. Since the momentum of C is antiparallel to the boost direction from the A to B rest frames, the C momentum in the B rest frame will be different, but it will still be antiparallel to this boost direction

$$\hat{z}_0^{\{B\}} = -\hat{p}_C^{\{B\}}. \tag{9}$$
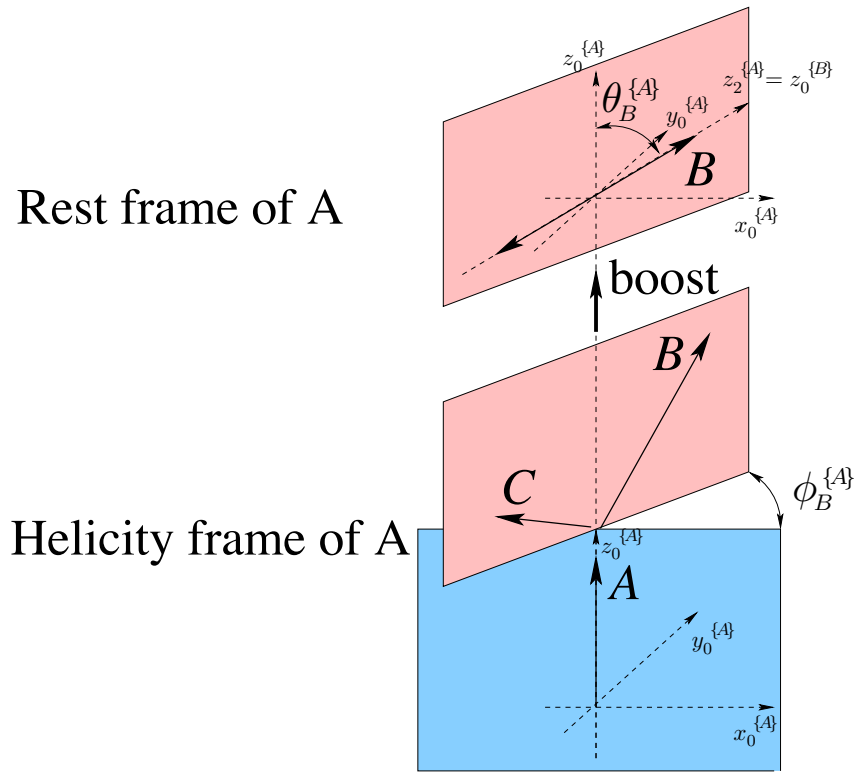
Figure 16: Coordinate axes for the spin quantization of particle A (bottom part), chosen to be the helicity frame of A ($\hat{z}_0 || \vec{p}_A$ in the rest frame of its parent particle or in the laboratory frame), together with the polar ($\theta_B^{\{A\}}$) and azimuthal ($\phi_B^{\{A\}}$) angles of the momentum of its child B in the A rest frame (top part). Notice that the directions of these coordinate axes, denoted as $\hat{x}_0^{\{A\}}$, $\hat{y}_0^{\{A\}}$, and $\hat{z}_0^{\{A\}}$, do not change when boosting from the helicity frame of A to its rest frame. After the Euler rotation $\mathcal{R}(\alpha = \phi_B^{\{A\}}, \beta = \theta_B^{\{A\}}, \gamma = 0)$ (see the text), the rotated z axis, $\hat{z}_2^{\{A\}}$, is aligned with the B momentum; thus the rotated coordinates become the helicity frame of B. If B has a sequential decay, then the same boost-rotation process is repeated to define the helicity frame for its decay products.

To determine $\hat{x}_0^{\{B\}}$ from Eq. (7), we need to find $\hat{x}_3^{\{A\}}$. After the first rotation by ϕ_B about $\hat{z}_0^{\{A\}}$, the $\hat{x}_1^{\{A\}}$ axis is along the component of $\vec{p}_B^{\{A\}}$ which is perpendicular to the $\hat{z}_0^{\{A\}}$ axis

$$\vec{a}_{B\perp z_0}^{\{A\}} \equiv (\vec{p}_B^{\{A\}})_{\perp \hat{z}_0^{\{A\}}} = \vec{p}_B^{\{A\}} - (\vec{p}_B^{\{A\}})_{\| \hat{z}_0^{\{A\}}},$$

$$= \vec{p}_B^{\{A\}} - (\vec{p}_B^{\{A\}} \cdot \hat{z}_0^{\{A\}})\, \hat{z}_0^{\{A\}},$$

$$\hat{x}_1^{\{A\}} = \hat{a}_{B\perp z_0}^{\{A\}} = \frac{\vec{a}_{B\perp z_0}^{\{A\}}}{|\vec{a}_{B\perp z_0}^{\{A\}}|}. \tag{10}$$

After the second rotation by θ_A about $\hat{y}_1^{\{A\}}$, $\hat{z}_2^{\{A\}} \equiv \hat{z}_3^{\{A\}} = \hat{p}_B^{\{A\}}$, and $\hat{x}_2^{\{A\}} = \hat{x}_3^{\{A\}}$ is antiparallel to the component of the $\hat{z}_0^{\{A\}}$ vector that is perpendicular to the new z axis *i.e.* $\hat{p}_B^{\{A\}}$. Thus

$$\vec{a}_{z_0 \perp B}^{\{A\}} \equiv (\hat{z}_0^{\{A\}})_{\perp \vec{p}_B^{\{A\}}} = \hat{z}_0^{\{A\}} - (\hat{z}_0^{\{A\}} \cdot \hat{p}_B^{\{A\}})\, \hat{p}_B^{\{A\}},$$

$$\hat{x}_0^{\{B\}} = \hat{x}_3^{\{A\}} = -\,\hat{a}_{z_0 \perp B}^{\{A\}} = -\,\frac{\vec{a}_{z_0 \perp B}^{\{A\}}}{|\vec{a}_{z_0 \perp B}^{\{A\}}|}. \tag{11}$$

Then we obtain $\hat{y}_0^{\{B\}} = \hat{z}_0^{\{B\}} \times \hat{x}_0^{\{B\}}$.

If C also decays, $C \to F\,G$, then the coordinates for the quantization of C spin in the C rest frame are defined by

$$\hat{z}_0^{\{C\}} = -\hat{z}_3^{\{A\}} = \hat{p}_C^{\{A\}} = -\hat{p}_B^{\{C\}}, \tag{12}$$

$$\hat{x}_0^{\{C\}} = \hat{x}_3^{\{A\}} = -\,\hat{a}_{z_0 \perp B}^{\{A\}} = +\hat{a}_{z_0 \perp C}^{\{A\}}, \tag{13}$$

$$\hat{y}_0^{\{C\}} = \hat{z}_0^{\{C\}} \times \hat{x}_0^{\{C\}}, \tag{14}$$

i.e. the z axis is reflected compared to the system used for the decay of particle B (it must point in the direction of C momentum in the A rest frame), but the x axis is kept the same, since we chose particle B for the rotation used in Eq. (5).

3.2   Matrix element for the Z_c^- decay chain

The decay matrix elements for the two interfering decay chains, $\Lambda_b^0 \to J/\psi\, N^*$, $N^* \to p\pi^-$ and $\Lambda_b^0 \to P_c^+ \pi^-$, $P_c^+ \to J/\psi\, p$ with $J/\psi \to \mu^+\mu^-$ in both cases, are identical to those used in the $\Lambda_b^0 \to J/\psi\, pK^-$ analysis [5], with K^- and Λ^* replaced by π^- and N^*. We now turn to the discussion of the additional interfering decay chain, $\Lambda_b^0 \to Z_{cf}\, p$, $Z_{cf} \to \psi\pi^-$ decays (denoting J/ψ as ψ), in which we allow more than one tetraquark state, $f = 1, 2, \ldots$. Superscripts containing the Z_c decay chain name without curly brackets, *e.g.* ϕ^{Z_c}, will denote quantities belonging to this decay chain and should not be confused with the superscript "$\{Z_c\}$" denoting the Z_c rest frame, *e.g.* $\phi^{\{Z_c\}}$. With only a few exceptions, we omit the N^* decay chain label. The angular calculations for the Z_c^- decay chain are analogous to that for P_c^+ by interchange of p and π^-, except for the angles to align the proton helicity.

The weak decay $\Lambda_b^0 \to Z_c f p$ is described by the term,

$$\mathcal{H}_{\lambda_{Z_c},\lambda_p^{Z_c}}^{\Lambda_b^0 \to Z_c f p} \, D_{\lambda_{\Lambda_b^0},\lambda_{Z_c}-\lambda_p^{Z_c}}^{\frac{1}{2}}(\phi_{Z_c}, \theta_{\Lambda_b^0}^{Z_c}, 0)^*, \tag{15}$$

where $\mathcal{H}_{\lambda_{Z_c},\lambda_p^{Z_c}}^{\Lambda_b^0 \to Z_c f p}$ are resonance (*i.e.* f) dependent helicity couplings. As for $|\lambda_{Z_c} - \lambda_p^{Z_c}| \leq \frac{1}{2}$, there are two different helicity couplings for $J_{Z_c} = 0$, and four for higher spin. The above mentioned ϕ_{Z_c}, $\theta_{\Lambda_b^0}^{Z_c}$ symbols refer to the azimuthal and polar angles of Z_c in the Λ_b^0 rest frame (see Fig. 17).

With the direction of Λ_b^0 in the lab frame $\hat{p}_{\Lambda_b^0}^{\{lab\}}$, and the direction of Z_c in the Λ_b^0 rest frame, the Λ_b^0 helicity angle in the Z_c decay chain can be calculated as,

$$\cos\theta_{\Lambda_b^0}^{Z_c} = \hat{p}_{\Lambda_b^0}^{\{lab\}} \cdot \hat{p}_{Z_c}^{\{\Lambda_b^0\}}. \tag{16}$$

The ϕ_{Z_c} angle cannot be set to zero, since we have already defined the $\hat{x}_0^{\{\Lambda_b^0\}}$ axis in the Λ_b^0 rest frame by the $\phi_{N^*} = 0$ convention:

$$\vec{a}_{N^*\perp z_0}^{\{\Lambda_b^0\}} = \vec{p}_{N^*}^{\{\Lambda_b^0\}} - (\vec{p}_{N^*}^{\{\Lambda_b^0\}} \cdot \hat{p}_{\Lambda_b^0}^{\{lab\}}) \, \hat{p}_{\Lambda_b^0}^{\{lab\}},$$

$$\hat{x}_0^{\{\Lambda_b^0\}} = \frac{\vec{a}_{N^*\perp z_0}^{\{\Lambda_b^0\}}}{|\vec{a}_{N^*\perp z_0}^{\{\Lambda_b^0\}}|}. \tag{17}$$

The ϕ_{Z_c} angle can be determined in the Λ_b^0 rest frame from

$$\phi_{Z_c} = \mathrm{atan2}\left((\hat{p}_{\Lambda_b^0}^{\{lab\}} \times \hat{x}_0^{\{\Lambda_b^0\}}) \cdot \hat{p}_{Z_c}^{\{\Lambda_b^0\}}, \, \hat{x}_0^{\{\Lambda_b^0\}} \cdot \hat{p}_{Z_c}^{\{\Lambda_b^0\}}\right). \tag{18}$$
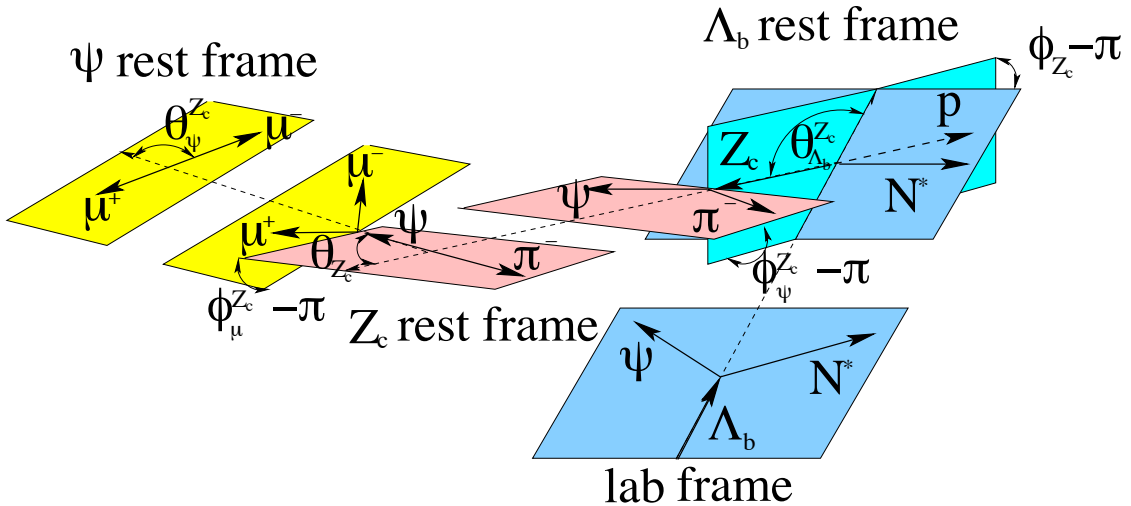

Figure 17: Definition of the decay angles in the Z_c^- decay chain.

The strong decay $Z_{cf} \to \psi\pi^-$ is described by a term

$$\mathcal{H}^{Z_{cf} \to \psi\pi}_{\lambda^{Z_c}_{\psi}} \; D^{J_{Z_{cf}}}_{\lambda_{Z_c}, \lambda^{Z_c}_{\psi}}(\phi^{Z_c}_{\psi}, \theta_{Z_c}, 0)^* \; R_{Z_{cf}}(M_{\psi\pi}), \tag{19}$$

where $\phi^{Z_c}_{\psi}, \theta_{Z_c}$ are the azimuthal and polar angles of the ψ in the Z_c rest frame (see Fig. 17). The $\hat{z}_0^{\{Z_c\}}$ direction is defined by the boost direction from the Λ_b^0 rest frame, which coincides with the $-\vec{p}_p^{\,\{Z_c\}}$ direction. This leads to

$$\cos\theta_{Z_c} = -\hat{p}_p^{\{Z_c\}} \cdot \hat{p}_{\psi}^{\{Z_c\}}. \tag{20}$$

The azimuthal angle of the ψ can now be determined in the Z_c rest frame (see Fig. 17) from

$$\phi^{Z_c}_{\psi} = \mathrm{atan2}\left(-(\hat{p}_p^{\{Z_c\}} \times \hat{x}_0^{\{Z_c\}}) \cdot \hat{p}_{\psi}^{\{Z_c\}}, \; \hat{x}_0^{\{Z_c\}} \cdot \hat{p}_{\psi}^{\{Z_c\}}\right). \tag{21}$$

The $\hat{x}_0^{\{Z_c\}}$ direction is defined by the convention that we used in the Λ_b^0 rest frame. Thus, we have

$$\vec{a}^{\{\Lambda_b^0\}}_{z_0 \perp Z_c} = \hat{p}_{\Lambda_b^0}^{\{lab\}} - (\hat{p}_{\Lambda_b^0}^{\{lab\}} \cdot \hat{p}_{Z_c}^{\{\Lambda_b^0\}}) \, \hat{p}_{Z_c}^{\{\Lambda_b^0\}},$$

$$\hat{x}_0^{\{Z_c\}} = -\frac{\vec{a}^{\{\Lambda_b^0\}}_{z_0 \perp Z_c}}{|\vec{a}^{\{\Lambda_b^0\}}_{z_0 \perp Z_c}|}. \tag{22}$$

Again, the ψ and p helicities are labeled as $\lambda^{Z_c}_{\psi}$ and $\lambda^{Z_c}_p$, with the Z_c superscript to make it clear that the spin quantization axes are different than in the N^* decay chain. Since the ψ is an intermediate particle, this has no consequences after we sum (coherently) over $\lambda^{Z_c}_{\psi} = -1, 0, +1$. The proton, however, is a final-state particle. Before the Z_c terms in the matrix element can be added coherently to the N^* terms, the $\lambda^{Z_c}_p$ states must be rotated to λ_p states (defined in the N^* decay chain). The proton helicity axes are different, since the proton comes from a decay of different particles in the two decay sequences, the N^* and Λ_b^0. The quantization axes are along the proton direction in the N^* and the Λ_b^0 rest frames, thus antiparallel to the particles recoiling against the proton: the π^- and Z_c, respectively. These directions are preserved when boosting to the proton rest frame. Thus, the polar angle between the two proton quantization axes ($\theta^{Z_c}_p$) can be determined from the opening angle between the π^- and Z_c mesons in the p rest frame,

$$\cos\theta^{Z_c}_p = \hat{p}_{\pi}^{\{p\}} \cdot \hat{p}_{Z_c}^{\{p\}}. \tag{23}$$

The dot product above must be calculated by operating on the $\vec{p}_{\pi}^{\,\{p\}}$ and $\vec{p}_{Z_c}^{\,\{p\}}$ vectors in the proton rest frame obtained by the same sequence of boost transformations, either according to the N^* or Z_c decay chains, or even by a direct boost transformation from the lab frame.

Unlike in the P_c decay chain, the azimuthal angle ($\alpha^{Z_c}_p$) aligning the two proton helicity frames is not zero. The angle can be determined from

$$\alpha_p^{Z_c} = \text{atan2}\left((\hat{z}_0^{\{p\}\ \Lambda_b^0} \times \hat{x}_0^{\{p\}\ \Lambda_b^0}) \cdot \hat{x}_0^{\{p\}\ N^*},\ \hat{x}_0^{\{p\}\ \Lambda_b^0} \cdot \hat{x}_0^{\{p\}\ N^*} \right), \tag{24}$$

where all vectors are in the p rest frame, $\hat{x}_0^{\{p\}\ N^*}$ is the direction of the x axis when boosting from the N^* rest frame, $\hat{x}_0^{\{p\}\ \Lambda_b^0}$ and $\hat{z}_0^{\{p\}\ \Lambda_b^0}$ are the directions of the x and z axes when boosting from the Λ_b^0 rest frame. From Eq. (9), $\hat{z}_0^{\{p\}\ \Lambda_b^0} = -\hat{p}_{Z_c}^{\{p\}}$. Direction of $\hat{x}_0^{\{p\}\ \Lambda_b^0}$ is given by Eq.(11) with $\hat{z}_0^{\{\Lambda_b^0\}} = \hat{p}_{\Lambda_b^0}^{\{\text{lab}\}}$

$$\vec{a}_{z_0 \perp Z_c}^{\{\Lambda_b^0\}} = \hat{p}_{\Lambda_b^0}^{\{\text{lab}\}} - (\hat{p}_{\Lambda_b^0}^{\{\text{lab}\}} \cdot \hat{p}_{Z_c}^{\{\Lambda_b^0\}}) \hat{p}_{Z_c}^{\{\Lambda_b^0\}},$$

$$\hat{x}_0^{\{p\}\ \Lambda_b^0} = \frac{\vec{a}_{z_0 \perp Z_c}^{\{\Lambda_b^0\}}}{|\vec{a}_{z_0 \perp Z_c}^{\{\Lambda_b^0\}}|}. \tag{25}$$

Therefore, the relation between λ_p and $\lambda_p^{Z_c}$ states is

$$|\lambda_p\rangle = \sum_{\lambda_p^{Z_c}} D_{\lambda_p^{Z_c}, \lambda_p}^{J_p}(\alpha_p^{Z_c}, \theta_p^{Z_c}, 0)^* |\lambda_p^{Z_c}\rangle = \sum_{\lambda_p^{Z_c}} e^{i\lambda_p^{Z_c} \alpha_p^{Z_c}} d_{\lambda_p^{Z_c}, \lambda_p}^{J_p}(\theta_p^{Z_c}) |\lambda_p^{Z_c}\rangle. \tag{26}$$

Thus, the term given by Eq. (19) must be preceded by

$$\sum_{\lambda_p^{Z_c} = \pm\frac{1}{2}} e^{i\lambda_p^{Z_c} \alpha_p^{Z_c}} d_{\lambda_p^{Z_c}, \lambda_p}^{J_p}(\theta_p^{Z_c}). \tag{27}$$

Parity conservation in $Z_{cf} \to \psi\pi^-$ decays leads to the following relation

$$\mathcal{H}_{-\lambda_\psi^{Z_c}}^{Z_{cf} \to \psi\pi} = P_\psi P_\pi P_{Z_{cf}} (-1)^{J_\psi + J_K - J_{Z_{cf}}} \mathcal{H}_{\lambda_\psi^{Z_c}}^{Z_{cf} \to \psi\pi}$$

$$= P_{Z_{cf}} (-1)^{1 - J_{Z_{cf}}} \mathcal{H}_{\lambda_\psi^{Z_c}}^{Z_{cf} \to \psi\pi}, \tag{28}$$

where $P_{Z_{cf}}$ is the parity of the Z_{cf} state. Then the number of independent helicity couplings to be determined from the data is reduced to two for $J_{Z_{cf}} \geq 1$ and remains equal to unity for $J_{Z_{cf}} = 0$. Since the helicity couplings enter the matrix element formula as a product, $\mathcal{H}_{\lambda_{Z_c}, \lambda_p^{Z_c}}^{\Lambda_b^0 \to Z_{cf}p} \mathcal{H}_{\lambda_\psi^{Z_c}}^{Z_{cf} \to \psi\pi}$, the relative magnitude and phase of these two sets must be fixed by a convention. For example, $\mathcal{H}_{\lambda_\psi^{Z_c} = 0}^{Z_{cf} \to \psi\pi}$ can be set to $(1, 0)$ for every Z_{cf} resonance, in which case $\mathcal{H}_{\lambda_\psi^{Z_c} = 1}^{Z_{cf} \to \psi\pi}$ develops a meaning of the complex ratio of $\mathcal{H}_{\lambda_\psi^{Z_c} = 1}^{Z_{cf} \to \psi\pi} / \mathcal{H}_{\lambda_\psi^{Z_c} = 0}^{Z_{cf} \to \psi\pi}$, while all $\mathcal{H}_{\lambda_{Z_c}, \lambda_p^{Z_c}}^{\Lambda_b^0 \to Z_{cf}p}$ couplings should have both real and imaginary parts free in the fit.

The term $R_{Z_{cf}}(M_{\psi\pi})$ in Eq. (19) describes the $\psi\pi$ invariant mass distribution of the Z_{cf} resonance. Angular momentum conservation restricts $\max(J_{Z_{cf}} - 1, 0) \leq L_{\Lambda_b^0}^{Z_{cf}} \leq J_{Z_{cf}} + 1$ in $\Lambda_b^0 \to Z_{cf}p$ decays. Angular momentum conservation also imposes $\max(|J_{Z_{cf}} - 1|, 0) \leq$

$L_{Z_{cf}} \leq J_{Z_{cf}} + 1$, which is further restricted by the parity conservation in the Z_{cf} decays, $P_{Z_{cf}} = (-1)^{L_{Z_{cf}}}$. We assume the minimal values of $L_{\Lambda_b^0}^{Z_{cf}}$ and of $L_{Z_{cf}}$ in $R_{Z_{cf}}(m_{\psi\pi})$.

The electromagnetic decay $\psi \to \mu^+\mu^-$ in the Z_c decay chain contributes a term

$$D^1_{\lambda_\psi^{Z_c}, \Delta\lambda_\mu^{Z_c}}(\phi_\mu^{Z_c}, \theta_\psi^{Z_c}, 0)^*. \tag{29}$$

The azimuthal and polar angle of the muon in the ψ rest frame, $\phi_\mu^{Z_c}$, $\theta_\psi^{Z_c}$, are different from ϕ_μ, θ_ψ introduced in the N^* decay chain. The ψ helicity axis is along the boost direction from the Z_c to the ψ rest frames, which is given by

$$\hat{z}_0^{\{\psi\}\ Z_c} = -\hat{p}_\pi^{\{\psi\}}, \tag{30}$$

and so

$$\cos\theta_\psi^{Z_c} = -\hat{p}_\pi^{\{\psi\}} \cdot \hat{p}_\mu^{\{\psi\}}. \tag{31}$$

The x axis is inherited from the Z_c rest frame (Eq. (11)),

$$\vec{a}_{z_0\perp\psi}^{\{Z_c\}} = -\vec{p}_p^{\{Z_c\}} + (\vec{p}_p^{\{Z_c\}} \cdot \hat{p}_\psi^{\{Z_c\}})\,\hat{p}_\psi^{\{Z_c\}}$$

$$\hat{x}_0^{\{\psi\}\ Z_c} = \hat{x}_3^{\{Z_c\}} = -\frac{\vec{a}_{z_0\perp\psi}^{\{Z_c\}}}{|\vec{a}_{z_0\perp\psi}^{\{Z_c\}}|}, \tag{32}$$

which leads to

$$\phi_\mu^{Z_c} = \text{atan2}\left(-(\hat{p}_\pi^{\{\psi\}} \times \hat{x}_0^{\{\psi\}\ Z_c}) \cdot \hat{p}_\mu^{\{\psi\}},\ \hat{x}_0^{\{\psi\}\ Z_c} \cdot \hat{p}_\mu^{\{\psi\}}\right). \tag{33}$$

The azimuthal angle $\alpha_\mu^{Z_c}$ is defined by

$$\alpha_\mu^{Z_c} = \text{atan2}\left((\hat{z}_3^{\{\psi\}\ Z_c} \times \hat{x}_3^{\{\psi\}\ Z_c}) \cdot \hat{x}_3^{\{\psi\}\ N^*},\ \hat{x}_3^{\{\psi\}\ Z_c} \cdot \hat{x}_3^{\{\psi\}\ N^*}\right), \tag{34}$$

where $\hat{z}_3^{\{\psi\}\ Z_c} = \hat{p}_\mu^{\{\psi\}\ Z_c}$, and from Eq. (11)

$$\hat{x}_3^{\{\psi\}\ Z_c} = -\hat{a}_{z_0\perp\mu}^{\{\psi\}\ Z_c}, \tag{35}$$

$$\vec{a}_{z_0\perp\mu}^{\{\psi\}\ Z_c} = -\hat{p}_\pi^{\{\psi\}} + (\hat{p}_\pi^{\{\psi\}} \cdot \hat{p}_\mu^{\{\psi\}})\,\hat{p}_\mu^{\{\psi\}}, \tag{36}$$

as well as

$$\hat{x}_3^{\{\psi\}\ N^*} = -\hat{a}_{z_0\perp\mu}^{\{\psi\}\ N^*}, \tag{37}$$

$$\vec{a}_{z_0\perp\mu}^{\{\psi\}\ N^*} = -\hat{p}_{N^*}^{\{\psi\}} + (\hat{p}_{N^*}^{\{\psi\}} \cdot \hat{p}_\mu^{\{\psi\}})\,\hat{p}_\mu^{\{\psi\}}. \tag{38}$$

Collecting terms from the three subsequent decays in the Z_c chain together,

$$\mathcal{M}^{Z_c}_{\lambda_{\Lambda_b^0}, \lambda_p^{Z_c}, \Delta\lambda_\mu^{Z_c}} = e^{i\lambda_{\Lambda_b^0}\phi_{Z_c}} \sum_f R_{Z_{cf}}(M_{\psi\pi}) \sum_{\lambda_\psi^{Z_c}} e^{i\lambda_\psi^{Z_c}\phi_\mu^{Z_c}}\, d^1_{\lambda_\psi^{Z_c}, \Delta\lambda_\mu}(\theta_\psi^{Z_c})$$

$$\times \sum_{\lambda_{Z_c}} \mathcal{H}^{\Lambda_b^0 \to Z_{cf}p}_{\lambda_{Z_c}, \lambda_p^{Z_c}}\, e^{i\lambda_{Z_c}\phi_\psi^{Z_c}}\, d^{\frac{1}{2}}_{\lambda_{\Lambda_b^0}, \lambda_{Z_c} - \lambda_p^{Z_c}}(\theta_{\Lambda_b^0}^{Z_c}) \mathcal{H}^{Z_{cf} \to \psi\pi}_{\lambda_\psi^{Z_c}}\, d^{J_{Z_{cf}}}_{\lambda_{Z_c}, \lambda_\psi^{Z_c}}(\theta_{Z_c}), \tag{39}$$

and adding them coherently to the N^* and the P_c matrix elements, via appropriate relations of $|\lambda_p\rangle|\lambda_{\mu^+}\rangle|\lambda_{\mu^-}\rangle$ to $|\lambda_p^{P_c}\rangle|\lambda_{\mu^+}^{P_c}\rangle|\lambda_{\mu^-}^{P_c}\rangle$ and $|\lambda_p^{Z_c}\rangle|\lambda_{\mu^+}^{Z_c}\rangle|\lambda_{\mu^-}^{Z_c}\rangle$ states as discussed above, leads to the final matrix element squared

$$
|\mathcal{M}|^2 = \sum_{\lambda_{\Lambda_b^0}=\pm\frac{1}{2}} \sum_{\lambda_p=\pm\frac{1}{2}} \sum_{\Delta\lambda_\mu=\pm 1} \left| \mathcal{M}^{N^*}_{\lambda_{\Lambda_b^0},\lambda_p,\Delta\lambda_\mu} + e^{i\,\Delta\lambda_\mu\alpha_\mu} \sum_{\lambda_p^{P_c}} d^{\frac{1}{2}}_{\lambda_p^{P_c},\lambda_p}(\theta_p)\, \mathcal{M}^{P_c}_{\lambda_{\Lambda_b^0},\lambda_p^{P_c},\Delta\lambda_\mu} \right.
$$
$$
\left. + e^{i\,\Delta\lambda_\mu\alpha_\mu^{Z_c}} \sum_{\lambda_p^{Z_c}} e^{i\lambda_p^{Z_c}\alpha_p^{Z_c}} d^{\frac{1}{2}}_{\lambda_p^{Z_c},\lambda_p}(\theta_p^{Z_c})\, \mathcal{M}^{Z_c}_{\lambda_{\Lambda_b^0},\lambda_p^{Z_c},\Delta\lambda_\mu} \right|^2 . \qquad (40)
$$

Assuming approximate CP symmetry, the helicity couplings for Λ_b^0 and $\overline{\Lambda}_b^0$ can be made equal, but the calculation of the angles requires some care, since parity (P) conservation does not change polar (*i.e.* helicity) angles, but does change azimuthal angles. Thus, not only must $\vec{p}_{\mu^+}$ be used instead of $\vec{p}_{\mu^-}$ for $\overline{\Lambda}_b^0$ candidates (with π^+ and $\bar{p}$ in the final state) in Eqs. (31), (33), and (34), but also all azimuthal angles must be reflected before entering the matrix element formula: $\phi_{Z_c} \to -\phi_{Z_c}$, $\phi_\psi^{Z_c} \to -\phi_\psi^{Z_c}$, $\phi_\mu^{Z_c} \to -\phi_\mu^{Z_c}$, $\alpha_p^{Z_c} \to -\alpha_p^{Z_c}$ and $\alpha_\mu^{Z_c} \to -\alpha_\mu^{Z_c}$ [25].

LHCb collaboration

R. Aaij[39], C. Abellán Beteta[41], B. Adeva[38], M. Adinolfi[47], Z. Ajaltouni[5], S. Akar[6], J. Albrecht[10], F. Alessio[39], M. Alexander[52], S. Ali[42], G. Alkhazov[31], P. Alvarez Cartelle[54], A.A. Alves Jr[58], S. Amato[2], S. Amerio[23], Y. Amhis[7], L. An[40], L. Anderlini[18], G. Andreassi[40], M. Andreotti[17,g], J.E. Andrews[59], R.B. Appleby[55], O. Aquines Gutierrez[11], F. Archilli[1], P. d'Argent[12], J. Arnau Romeu[6], A. Artamonov[36], M. Artuso[60], E. Aslanides[6], G. Auriemma[26,s], M. Baalouch[5], S. Bachmann[12], J.J. Back[49], A. Badalov[37], C. Baesso[61], W. Baldini[17], R.J. Barlow[55], C. Barschel[39], S. Barsuk[7], W. Barter[39], V. Batozskaya[29], V. Battista[40], A. Bay[40], L. Beaucourt[4], J. Beddow[52], F. Bedeschi[24], I. Bediaga[1], L.J. Bel[42], V. Bellee[40], N. Belloli[21,i], K. Belous[36], I. Belyaev[32], E. Ben-Haim[8], G. Bencivenni[19], S. Benson[39], J. Benton[47], A. Berezhnoy[33], R. Bernet[41], A. Bertolin[23], M.-O. Bettler[39], M. van Beuzekom[42], S. Bifani[46], P. Billoir[8], T. Bird[55], A. Birnkraut[10], A. Bitadze[55], A. Bizzeti[18,u], T. Blake[49], F. Blanc[40], J. Blouw[11], S. Blusk[60], V. Bocci[26], T. Boettcher[57], A. Bondar[35], N. Bondar[31,39], W. Bonivento[16], S. Borghi[55], M. Borisyak[67], M. Borsato[38], F. Bossu[7], M. Boubdir[9], T.J.V. Bowcock[53], E. Bowen[41], C. Bozzi[17,39], S. Braun[12], M. Britsch[12], T. Britton[60], J. Brodzicka[55], E. Buchanan[47], C. Burr[55], A. Bursche[2], J. Buytaert[39], S. Cadeddu[16], R. Calabrese[17,g], M. Calvi[21,i], M. Calvo Gomez[37,m], P. Campana[19], D. Campora Perez[39], L. Capriotti[55], A. Carbone[15,e], G. Carboni[25,j], R. Cardinale[20,h], A. Cardini[16], P. Carniti[21,i], L. Carson[51], K. Carvalho Akiba[2], G. Casse[53], L. Cassina[21,i], L. Castillo Garcia[40], M. Cattaneo[39], Ch. Cauet[10], G. Cavallero[20], R. Cenci[24,t], M. Charles[8], Ph. Charpentier[39], G. Chatzikonstantinidis[46], M. Chefdeville[4], S. Chen[55], S.-F. Cheung[56], V. Chobanova[38], M. Chrzaszcz[41,27], X. Cid Vidal[38], G. Ciezarek[42], P.E.L. Clarke[51], M. Clemencic[39], H.V. Cliff[48], J. Closier[39], V. Coco[58], J. Cogan[6], E. Cogneras[5], V. Cogoni[16,f], L. Cojocariu[30], G. Collazuol[23,o], P. Collins[39], A. Comerma-Montells[12], A. Contu[39], A. Cook[47], S. Coquereau[8], G. Corti[39], M. Corvo[17,g], C.M. Costa Sobral[49], B. Couturier[39], G.A. Cowan[51], D.C. Craik[51], A. Crocombe[49], M. Cruz Torres[61], S. Cunliffe[54], R. Currie[54], C. D'Ambrosio[39], E. Dall'Occo[42], J. Dalseno[47], P.N.Y. David[42], A. Davis[58], O. De Aguiar Francisco[2], K. De Bruyn[6], S. De Capua[55], M. De Cian[12], J.M. De Miranda[1], L. De Paula[2], P. De Simone[19], C.-T. Dean[52], D. Decamp[4], M. Deckenhoff[10], L. Del Buono[8], M. Demmer[10], D. Derkach[67], O. Deschamps[5], F. Dettori[39], B. Dey[22], A. Di Canto[39], H. Dijkstra[39], F. Dordei[39], M. Dorigo[40], A. Dosil Suárez[38], A. Dovbnya[44], K. Dreimanis[53], L. Dufour[42], G. Dujany[55], K. Dungs[39], P. Durante[39], R. Dzhelyadin[36], A. Dziurda[39], A. Dzyuba[31], N. Déléage[4], S. Easo[50], U. Egede[54], V. Egorychev[32], S. Eidelman[35], S. Eisenhardt[51], U. Eitschberger[10], R. Ekelhof[10], L. Eklund[52], Ch. Elsasser[41], S. Ely[60], S. Esen[12], H.M. Evans[48], T. Evans[56], A. Falabella[15], N. Farley[46], S. Farry[53], R. Fay[53], D. Ferguson[51], V. Fernandez Albor[38], F. Ferrari[15,39], F. Ferreira Rodrigues[1], M. Ferro-Luzzi[39], S. Filippov[34], M. Fiore[17,g], M. Fiorini[17,g], M. Firlej[28], C. Fitzpatrick[40], T. Fiutowski[28], F. Fleuret[7,b], K. Fohl[39], M. Fontana[16], F. Fontanelli[20,h], D.C. Forshaw[60], R. Forty[39], M. Frank[39], C. Frei[39], M. Frosini[18], J. Fu[22,q], E. Furfaro[25,j], C. Färber[39], A. Gallas Torreira[38], D. Galli[15,e], S. Gallorini[23], S. Gambetta[51], M. Gandelman[2], P. Gandini[56], Y. Gao[3], J. García Pardiñas[38], J. Garra Tico[48], L. Garrido[37], P.J. Garsed[48], D. Gascon[37], C. Gaspar[39], L. Gavardi[10], G. Gazzoni[5], D. Gerick[12], E. Gersabeck[12], M. Gersabeck[55], T. Gershon[49], Ph. Ghez[4], S. Gianì[40], V. Gibson[48], O.G. Girard[40], L. Giubega[30], K. Gizdov[51], V.V. Gligorov[8], D. Golubkov[32], A. Golutvin[54,39], A. Gomes[1,a], I.V. Gorelov[33], C. Gotti[21,i], M. Grabalosa Gándara[5], R. Graciani Diaz[37], L.A. Granado Cardoso[39], E. Graugés[37], E. Graverini[41], G. Graziani[18], A. Grecu[30], P. Griffith[46], L. Grillo[12], B.R. Gruberg Cazon[56], O. Grünberg[65], E. Gushchin[34],

Yu. Guz[36], T. Gys[39], C. Göbel[61], T. Hadavizadeh[56], C. Hadjivasiliou[60], G. Haefeli[40], C. Haen[39], S.C. Haines[48], S. Hall[54], B. Hamilton[59], X. Han[12], S. Hansmann-Menzemer[12], N. Harnew[56], S.T. Harnew[47], J. Harrison[55], J. He[39], T. Head[40], A. Heister[9], K. Hennessy[53], P. Henrard[5], L. Henry[8], J.A. Hernando Morata[38], E. van Herwijnen[39], M. Heß[65], A. Hicheur[2], D. Hill[56], C. Hombach[55], W. Hulsbergen[42], T. Humair[54], M. Hushchyn[67], N. Hussain[56], D. Hutchcroft[53], M. Idzik[28], P. Ilten[57], R. Jacobsson[39], A. Jaeger[12], J. Jalocha[56], E. Jans[42], A. Jawahery[59], M. John[56], D. Johnson[39], C.R. Jones[48], C. Joram[39], B. Jost[39], N. Jurik[60], S. Kandybei[44], W. Kanso[6], M. Karacson[39], J.M. Kariuki[47], S. Karodia[52], M. Kecke[12], M. Kelsey[60], I.R. Kenyon[46], M. Kenzie[39], T. Ketel[43], E. Khairullin[67], B. Khanji[21,39,i], C. Khurewathanakul[40], T. Kirn[9], S. Klaver[55], K. Klimaszewski[29], S. Koliiev[45], M. Kolpin[12], I. Komarov[40], R.F. Koopman[43], P. Koppenburg[42], A. Kozachuk[33], M. Kozeiha[5], L. Kravchuk[34], K. Kreplin[12], M. Kreps[49], P. Krokovny[35], F. Kruse[10], W. Krzemien[29], W. Kucewicz[27,l], M. Kucharczyk[27], V. Kudryavtsev[35], A.K. Kuonen[40], K. Kurek[29], T. Kvaratskheliya[32,39], D. Lacarrere[39], G. Lafferty[55,39], A. Lai[16], D. Lambert[51], G. Lanfranchi[19], C. Langenbruch[49], B. Langhans[39], T. Latham[49], C. Lazzeroni[46], R. Le Gac[6], J. van Leerdam[42], J.-P. Lees[4], A. Leflat[33,39], J. Lefrançois[7], R. Lefèvre[5], F. Lemaitre[39], E. Lemos Cid[38], O. Leroy[6], T. Lesiak[27], B. Leverington[12], Y. Li[7], T. Likhomanenko[67,66], R. Lindner[39], C. Linn[39], F. Lionetto[41], B. Liu[16], X. Liu[3], D. Loh[49], I. Longstaff[52], J.H. Lopes[2], D. Lucchesi[23,o], M. Lucio Martinez[38], H. Luo[51], A. Lupato[23], E. Luppi[17,g], O. Lupton[56], A. Lusiani[24], X. Lyu[62], F. Machefert[7], F. Maciuc[30], O. Maev[31], K. Maguire[55], S. Malde[56], A. Malinin[66], T. Maltsev[35], G. Manca[7], G. Mancinelli[6], P. Manning[60], J. Maratas[5], J.F. Marchand[4], U. Marconi[15], C. Marin Benito[37], P. Marino[24,t], J. Marks[12], G. Martellotti[26], M. Martin[6], M. Martinelli[40], D. Martinez Santos[38], F. Martinez Vidal[68], D. Martins Tostes[2], L.M. Massacrier[7], A. Massafferri[1], R. Matev[39], A. Mathad[49], Z. Mathe[39], C. Matteuzzi[21], A. Mauri[41], B. Maurin[40], A. Mazurov[46], M. McCann[54], J. McCarthy[46], A. McNab[55], R. McNulty[13], B. Meadows[58], F. Meier[10], M. Meissner[12], D. Melnychuk[29], M. Merk[42], E Michielin[23], D.A. Milanes[64], M.-N. Minard[4], D.S. Mitzel[12], J. Molina Rodriguez[61], I.A. Monroy[64], S. Monteil[5], M. Morandin[23], P. Morawski[28], A. Mordà[6], M.J. Morello[24,t], J. Moron[28], A.B. Morris[51], R. Mountain[60], F. Muheim[51], M Mulder[42], M. Mussini[15], D. Müller[55], J. Müller[10], K. Müller[41], V. Müller[10], P. Naik[47], T. Nakada[40], R. Nandakumar[50], A. Nandi[56], I. Nasteva[2], M. Needham[51], N. Neri[22], S. Neubert[12], N. Neufeld[39], M. Neuner[12], A.D. Nguyen[40], C. Nguyen-Mau[40,n], V. Niess[5], S. Nieswand[9], R. Niet[10], N. Nikitin[33], T. Nikodem[12], A. Novoselov[36], D.P. O'Hanlon[49], A. Oblakowska-Mucha[28], V. Obraztsov[36], S. Ogilvy[19], O. Okhrimenko[45], R. Oldeman[48], C.J.G. Onderwater[69], J.M. Otalora Goicochea[2], A. Otto[39], P. Owen[54], A. Oyanguren[68], P.R. Pais[40], A. Palano[14,d], F. Palombo[22,q], M. Palutan[19], J. Panman[39], A. Papanestis[50], M. Pappagallo[52], L.L. Pappalardo[17,g], C. Pappenheimer[58], W. Parker[59], C. Parkes[55], G. Passaleva[18], G.D. Patel[53], M. Patel[54], C. Patrignani[15,e], A. Pearce[55,50], A. Pellegrino[42], G. Penso[26,k], M. Pepe Altarelli[39], S. Perazzini[39], P. Perret[5], L. Pescatore[46], K. Petridis[47], A. Petrolini[20,h], A. Petrov[66], M. Petruzzo[22,q], E. Picatoste Olloqui[37], B. Pietrzyk[4], M. Pikies[27], D. Pinci[26], A. Pistone[20], A. Piucci[12], S. Playfer[51], M. Plo Casasus[38], T. Poikela[39], F. Polci[8], A. Poluektov[49,35], I. Polyakov[32], E. Polycarpo[2], G.J. Pomery[47], A. Popov[36], D. Popov[11,39], B. Popovici[30], C. Potterat[2], E. Price[47], J.D. Price[53], J. Prisciandaro[38], A. Pritchard[53], C. Prouve[47], V. Pugatch[45], A. Puig Navarro[40], G. Punzi[24,p], W. Qian[56], R. Quagliani[7,47], B. Rachwal[27], J.H. Rademacker[47], M. Rama[24], M. Ramos Pernas[38], M.S. Rangel[2], I. Raniuk[44], G. Raven[43], F. Redi[54], S. Reichert[10], A.C. dos Reis[1], C. Remon Alepuz[68], V. Renaudin[7], S. Ricciardi[50], S. Richards[47], M. Rihl[39], K. Rinnert[53,39], V. Rives Molina[37], P. Robbe[7],

A.B. Rodrigues[1], E. Rodrigues[58], J.A. Rodriguez Lopez[64], P. Rodriguez Perez[55],
A. Rogozhnikov[67], S. Roiser[39], V. Romanovskiy[36], A. Romero Vidal[38], J.W. Ronayne[13],
M. Rotondo[23], T. Ruf[39], P. Ruiz Valls[68], J.J. Saborido Silva[38], E. Sadykhov[32], N. Sagidova[31],
B. Saitta[16,f], V. Salustino Guimaraes[2], C. Sanchez Mayordomo[68], B. Sanmartin Sedes[38],
R. Santacesaria[26], C. Santamarina Rios[38], M. Santimaria[19], E. Santovetti[25,j], A. Sarti[19,k],
C. Satriano[26,s], A. Satta[25], D.M. Saunders[47], D. Savrina[32,33], S. Schael[9], M. Schiller[39],
H. Schindler[39], M. Schlupp[10], M. Schmelling[11], T. Schmelzer[10], B. Schmidt[39], O. Schneider[40],
A. Schopper[39], M. Schubiger[40], M.-H. Schune[7], R. Schwemmer[39], B. Sciascia[19], A. Sciubba[26,k],
A. Semennikov[32], A. Sergi[46], N. Serra[41], J. Serrano[6], L. Sestini[23], P. Seyfert[21], M. Shapkin[36],
I. Shapoval[17,44,g], Y. Shcheglov[31], T. Shears[53], L. Shekhtman[35], V. Shevchenko[66], A. Shires[10],
B.G. Siddi[17], R. Silva Coutinho[41], L. Silva de Oliveira[2], G. Simi[23,o], M. Sirendi[48],
N. Skidmore[47], T. Skwarnicki[60], E. Smith[54], I.T. Smith[51], J. Smith[48], M. Smith[55], H. Snoek[42],
M.D. Sokoloff[58], F.J.P. Soler[52], D. Souza[47], B. Souza De Paula[2], B. Spaan[10], P. Spradlin[52],
S. Sridharan[39], F. Stagni[39], M. Stahl[12], S. Stahl[39], P. Stefko[40], S. Stefkova[54], O. Steinkamp[41],
O. Stenyakin[36], S. Stevenson[56], S. Stoica[30], S. Stone[60], B. Storaci[41], S. Stracka[24,t],
M. Straticiuc[30], U. Straumann[41], L. Sun[58], W. Sutcliffe[54], K. Swientek[28], V. Syropoulos[43],
M. Szczekowski[29], T. Szumlak[28], S. T'Jampens[4], A. Tayduganov[6], T. Tekampe[10],
G. Tellarini[17,g], F. Teubert[39], C. Thomas[56], E. Thomas[39], J. van Tilburg[42], V. Tisserand[4],
M. Tobin[40], S. Tolk[48], L. Tomassetti[17,g], D. Tonelli[39], S. Topp-Joergensen[56], F. Toriello[60],
E. Tournefier[4], S. Tourneur[40], K. Trabelsi[40], M. Traill[52], M.T. Tran[40], M. Tresch[41],
A. Trisovic[39], A. Tsaregorodtsev[6], P. Tsopelas[42], A. Tully[48], N. Tuning[42], A. Ukleja[29],
A. Ustyuzhanin[67,66], U. Uwer[12], C. Vacca[16,39,f], V. Vagnoni[15,39], S. Valat[39], G. Valenti[15],
A. Vallier[7], R. Vazquez Gomez[19], P. Vazquez Regueiro[38], S. Vecchi[17], M. van Veghel[42],
J.J. Velthuis[47], M. Veltri[18,r], G. Veneziano[40], A. Venkateswaran[60], M. Vesterinen[12], B. Viaud[7],
D. Vieira[1], M. Vieites Diaz[38], X. Vilasis-Cardona[37,m], V. Volkov[33], A. Vollhardt[41], B Voneki[39],
D. Voong[47], A. Vorobyev[31], V. Vorobyev[35], C. Voß[65], J.A. de Vries[42], C. Vázquez Sierra[38],
R. Waldi[65], C. Wallace[49], R. Wallace[13], J. Walsh[24], J. Wang[60], D.R. Ward[48], H.M. Wark[53],
N.K. Watson[46], D. Websdale[54], A. Weiden[41], M. Whitehead[39], J. Wicht[49], G. Wilkinson[56,39],
M. Wilkinson[60], M. Williams[39], M.P. Williams[46], M. Williams[57], T. Williams[46], F.F. Wilson[50],
J. Wimberley[59], J. Wishahi[10], W. Wislicki[29], M. Witek[27], G. Wormser[7], S.A. Wotton[48],
K. Wraight[52], S. Wright[48], K. Wyllie[39], Y. Xie[63], Z. Xu[40], Z. Yang[3], H. Yin[63], J. Yu[63],
X. Yuan[35], O. Yushchenko[36], M. Zangoli[15], K.A. Zarebski[46], M. Zavertyaev[11,c], L. Zhang[3],
Y. Zhang[7], Y. Zhang[62], A. Zhelezov[12], Y. Zheng[62], A. Zhokhov[32], V. Zhukov[9], S. Zucchelli[15].

[1]*Centro Brasileiro de Pesquisas Físicas (CBPF), Rio de Janeiro, Brazil*
[2]*Universidade Federal do Rio de Janeiro (UFRJ), Rio de Janeiro, Brazil*
[3]*Center for High Energy Physics, Tsinghua University, Beijing, China*
[4]*LAPP, Université Savoie Mont-Blanc, CNRS/IN2P3, Annecy-Le-Vieux, France*
[5]*Clermont Université, Université Blaise Pascal, CNRS/IN2P3, LPC, Clermont-Ferrand, France*
[6]*CPPM, Aix-Marseille Université, CNRS/IN2P3, Marseille, France*
[7]*LAL, Université Paris-Sud, CNRS/IN2P3, Orsay, France*
[8]*LPNHE, Université Pierre et Marie Curie, Université Paris Diderot, CNRS/IN2P3, Paris, France*
[9]*I. Physikalisches Institut, RWTH Aachen University, Aachen, Germany*
[10]*Fakultät Physik, Technische Universität Dortmund, Dortmund, Germany*
[11]*Max-Planck-Institut für Kernphysik (MPIK), Heidelberg, Germany*
[12]*Physikalisches Institut, Ruprecht-Karls-Universität Heidelberg, Heidelberg, Germany*
[13]*School of Physics, University College Dublin, Dublin, Ireland*
[14]*Sezione INFN di Bari, Bari, Italy*

[15]*Sezione INFN di Bologna, Bologna, Italy*
[16]*Sezione INFN di Cagliari, Cagliari, Italy*
[17]*Sezione INFN di Ferrara, Ferrara, Italy*
[18]*Sezione INFN di Firenze, Firenze, Italy*
[19]*Laboratori Nazionali dell'INFN di Frascati, Frascati, Italy*
[20]*Sezione INFN di Genova, Genova, Italy*
[21]*Sezione INFN di Milano Bicocca, Milano, Italy*
[22]*Sezione INFN di Milano, Milano, Italy*
[23]*Sezione INFN di Padova, Padova, Italy*
[24]*Sezione INFN di Pisa, Pisa, Italy*
[25]*Sezione INFN di Roma Tor Vergata, Roma, Italy*
[26]*Sezione INFN di Roma La Sapienza, Roma, Italy*
[27]*Henryk Niewodniczanski Institute of Nuclear Physics Polish Academy of Sciences, Kraków, Poland*
[28]*AGH - University of Science and Technology, Faculty of Physics and Applied Computer Science, Kraków, Poland*
[29]*National Center for Nuclear Research (NCBJ), Warsaw, Poland*
[30]*Horia Hulubei National Institute of Physics and Nuclear Engineering, Bucharest-Magurele, Romania*
[31]*Petersburg Nuclear Physics Institute (PNPI), Gatchina, Russia*
[32]*Institute of Theoretical and Experimental Physics (ITEP), Moscow, Russia*
[33]*Institute of Nuclear Physics, Moscow State University (SINP MSU), Moscow, Russia*
[34]*Institute for Nuclear Research of the Russian Academy of Sciences (INR RAN), Moscow, Russia*
[35]*Budker Institute of Nuclear Physics (SB RAS) and Novosibirsk State University, Novosibirsk, Russia*
[36]*Institute for High Energy Physics (IHEP), Protvino, Russia*
[37]*Universitat de Barcelona, Barcelona, Spain*
[38]*Universidad de Santiago de Compostela, Santiago de Compostela, Spain*
[39]*European Organization for Nuclear Research (CERN), Geneva, Switzerland*
[40]*Ecole Polytechnique Fédérale de Lausanne (EPFL), Lausanne, Switzerland*
[41]*Physik-Institut, Universität Zürich, Zürich, Switzerland*
[42]*Nikhef National Institute for Subatomic Physics, Amsterdam, The Netherlands*
[43]*Nikhef National Institute for Subatomic Physics and VU University Amsterdam, Amsterdam, The Netherlands*
[44]*NSC Kharkiv Institute of Physics and Technology (NSC KIPT), Kharkiv, Ukraine*
[45]*Institute for Nuclear Research of the National Academy of Sciences (KINR), Kyiv, Ukraine*
[46]*University of Birmingham, Birmingham, United Kingdom*
[47]*H.H. Wills Physics Laboratory, University of Bristol, Bristol, United Kingdom*
[48]*Cavendish Laboratory, University of Cambridge, Cambridge, United Kingdom*
[49]*Department of Physics, University of Warwick, Coventry, United Kingdom*
[50]*STFC Rutherford Appleton Laboratory, Didcot, United Kingdom*
[51]*School of Physics and Astronomy, University of Edinburgh, Edinburgh, United Kingdom*
[52]*School of Physics and Astronomy, University of Glasgow, Glasgow, United Kingdom*
[53]*Oliver Lodge Laboratory, University of Liverpool, Liverpool, United Kingdom*
[54]*Imperial College London, London, United Kingdom*
[55]*School of Physics and Astronomy, University of Manchester, Manchester, United Kingdom*
[56]*Department of Physics, University of Oxford, Oxford, United Kingdom*
[57]*Massachusetts Institute of Technology, Cambridge, MA, United States*
[58]*University of Cincinnati, Cincinnati, OH, United States*
[59]*University of Maryland, College Park, MD, United States*
[60]*Syracuse University, Syracuse, NY, United States*
[61]*Pontifícia Universidade Católica do Rio de Janeiro (PUC-Rio), Rio de Janeiro, Brazil, associated to [2]*
[62]*University of Chinese Academy of Sciences, Beijing, China, associated to [3]*
[63]*Institute of Particle Physics, Central China Normal University, Wuhan, Hubei, China, associated to [3]*
[64]*Departamento de Fisica , Universidad Nacional de Colombia, Bogota, Colombia, associated to [8]*

[65] *Institut für Physik, Universität Rostock, Rostock, Germany, associated to [12]*

[66] *National Research Centre Kurchatov Institute, Moscow, Russia, associated to [32]*

[67] *Yandex School of Data Analysis, Moscow, Russia, associated to [32]*

[68] *Instituto de Fisica Corpuscular (IFIC), Universitat de Valencia-CSIC, Valencia, Spain, associated to [37]*

[69] *Van Swinderen Institute, University of Groningen, Groningen, The Netherlands, associated to [42]*

[a] *Universidade Federal do Triângulo Mineiro (UFTM), Uberaba-MG, Brazil*

[b] *Laboratoire Leprince-Ringuet, Palaiseau, France*

[c] *P.N. Lebedev Physical Institute, Russian Academy of Science (LPI RAS), Moscow, Russia*

[d] *Università di Bari, Bari, Italy*

[e] *Università di Bologna, Bologna, Italy*

[f] *Università di Cagliari, Cagliari, Italy*

[g] *Università di Ferrara, Ferrara, Italy*

[h] *Università di Genova, Genova, Italy*

[i] *Università di Milano Bicocca, Milano, Italy*

[j] *Università di Roma Tor Vergata, Roma, Italy*

[k] *Università di Roma La Sapienza, Roma, Italy*

[l] *AGH - University of Science and Technology, Faculty of Computer Science, Electronics and Telecommunications, Kraków, Poland*

[m] *LIFAELS, La Salle, Universitat Ramon Llull, Barcelona, Spain*

[n] *Hanoi University of Science, Hanoi, Viet Nam*

[o] *Università di Padova, Padova, Italy*

[p] *Università di Pisa, Pisa, Italy*

[q] *Università degli Studi di Milano, Milano, Italy*

[r] *Università di Urbino, Urbino, Italy*

[s] *Università della Basilicata, Potenza, Italy*

[t] *Scuola Normale Superiore, Pisa, Italy*

[u] *Università di Modena e Reggio Emilia, Modena, Italy*